University of Glasgow

DEPARTMENT OF

AEROSPACE ENGINEERING

Simulation of Helicopter Manoeuvres Using an Individual Blade Rotor Model.

David Anderson
Postgraduate Researcher

Internal Report No 9514

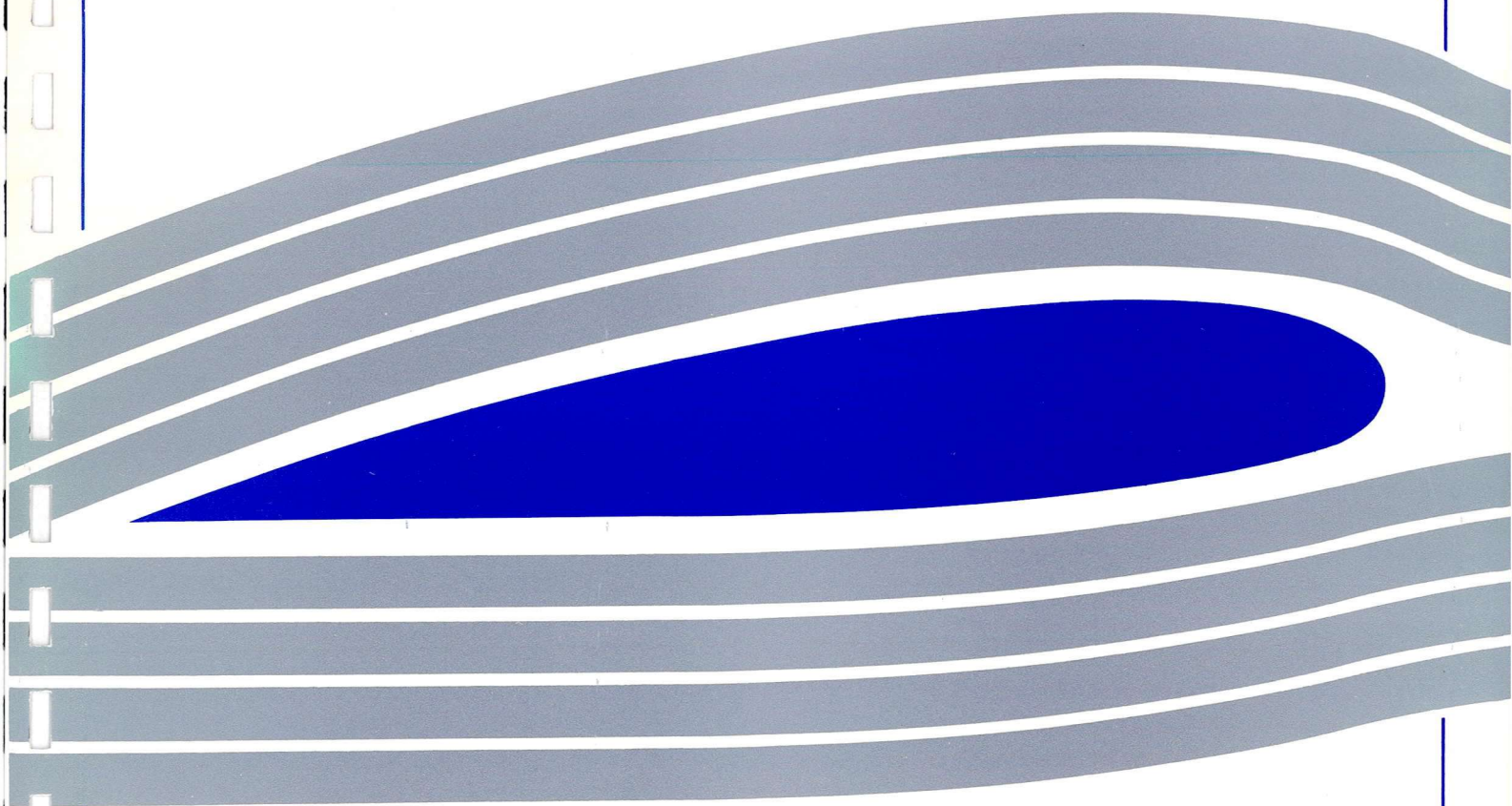

Simulation of Helicopter Manoeuvres Using an Individual Blade Rotor Model.

David Anderson
Postgraduate Researcher
Internal Report No 9514

Department of Aerospace Engineering
University of Glasgow
Glasgow

Abstract

A control methodology is presented and applied to the simulation of helicopter manoeuvres using an individual blade rotor model. The novelty of constraining an individual blade/blade element rotorcraft model is explained with reference to some existing manoeuvre simulation techniques. A fully non-linear control algorithm is employed which estimates the controls required to maintain a constant flight path by minimising the error between the inertial frame flight path states predicted by the rotorcraft model, and those demanded by the flight path generator. A simple flight path generation model, based on Newtonian kinematics is used. Firstly, the algorithm is evaluated in a disturbance rejection role, negating the effect of obstruction-induced atmospheric turbulence. Secondly, a flare to hover manoeuvre is simulated and the results discussed. The effects of parameter changes within the control algorithm are also discussed and the results for changes in tolerance levels and the control application interval are presented. Finally an approach to an offshore oil platform, landing on the helideck, with the turbulence field included was performed. It is found that the control algorithm tracks the required flight path well in both still air and turbulence.

Nomenclature.

Control Algorithm Parameters

$E(\mathbf{u}(t_k))$	output error vector .
$G(.)$	mapping from input-output space.
$J[]$	jacobian matrix.
$\mathbf{u}(t_k)$	input (control) vector at time t_k.
$\underline{\mathbf{X}}$	system state vector.
$\underline{\hat{\mathbf{X}}}$	observer state vector.
$\mathbf{y}(t_k)$	output vector at time t_k.
$\mathbf{y}_{DES}$	desired output vector.
STD	standard deviation of the i^{th} variable.
CSTD	cumulative standard deviation coefficient.
T	control application interval.

Rotorcraft Model Parameters.

u,v,w	translational velocities (body axes).
$\dot{u}$, $\dot{v}$, $\dot{w}$	body accelerations.
x_e, y_e, z_e	c.g. position in x,y,z-dir.^{ns} (inertial frame).
p,q,r	Angular rates about the c.g. (body axes).
ϕ, θ, ψ	Euler angles.
θ_0	Main rotor collective pitch.
θ_{1s}	Main rotor longitudinal cyclic pitch.
θ_{1c}	Main rotor lateral cyclic pitch.
θ_{tr}	Tail rotor collective pitch.

FPG model parameters.

a_x, a_z	Desired longitudinal accelerations.
u_x, u_z	Trim inertial velocities.
s_z	Tuned initial altitude.

1.0 Introduction.

This research at the Aerospace Dept. of the University of Glasgow has been concerned with the simulation of flight past obstacles in a realistic atmospheric environment. Situations as varied as low altitude, close proximity flight near to a tower block, to flight over a clifftop for air/sea rescue missions, to making an approach to a north sea oil platform are common operational environments for many types of helicopter. A realistic, but simple model of the turbulence induced by the flow obstruction would therefore be regarded as a valuable design tool, allowing accurate manoeuvre simulation as well as stability, control authority and operational viability analysis.

Modelling of the turbulent wake induced by the presence of an obstacle in the flow field was accomplished using a commercial CFD package, (FLUENT). Using a discrete field for gust modelling enables the accurate repetition of numerical experiments for different flight conditions by using absolute rather than statistically equivalent turbulent velocity data. However, only a finite turbulence field can be incorporated into the rotorcraft simulation and should a divergent rigid body mode be excited, colliding with the obstacle or exceeding the field boundary becomes a realistic possibility. It was therefore necessary for repeatability and consistency that a controller be developed which would negate the effect of atmospheric disturbance on the low frequency, rigid body modes, so maintaining a constant flight path. Due to the success of the control algorithm in the disturbance rejection role, it was proposed to extend the application of the controller to the simulation of rudimentary helicopter manoeuvres.

Simulation of helicopter manoeuvres has recently been accomplished using Inverse Simulation, a technique whereby the controls required to perform a predefined manoeuvre are calculated, enabling control authority analysis to be enacted. Although no control law is used explicitly, the method for constraining the flight path is of interest. Continual adjustments are made to the control vector such that the equation,

$$G\left(\mathbf{u}(t)\right) - \mathbf{y}_{DES}(t) = 0 \qquad \text{Eqn}(1.1)$$

is minimised, Ref(1). Inverse simulation algorithms such as GENISA (GENeric Inverse Simulation Algorithm), developed by Rutherford and Thomson, Ref(2), use Newton-Raphson iteration (generally regarded as the most powerful technique for

solving problems such as eq(1.1)) for control modification. GENISA was used in the current work as a tool to provide the control displacements necessary to fulfil the control algorithm requirements.

In the past, an actuator disc (disc model) was used in inverse simulation to model the helicopter rotor forces and moments, mainly due to limitations in the computing power available. Using a disc model representation causes the rotor to act as a low pass filter to the minimisation algorithm, preventing the transfer of vibration or the effects of other high frequency inputs from having any effect on the solution. Atmospheric turbulence, for example, introduces additional loads on the aircraft, directly affecting all the dynamic modes operating within a wide frequency bandwidth - especially the rotor modes at (N/rev, N±1/rev) which may be primarily responsible for gust induced vibration, Ref.(3). By using a fully coupled, articulated, individual blade-blade element model these modes are transmitted to the fuselage and are therefore present in the control selection algorithm. Thus, using a blade element model yields a more realistic representation of the overall change in the aircraft due to atmospheric uncertainties. The simulation is further enhanced by the use of an individual blade tail rotor in the simulation, rarely, if ever, used in control law design.

In situations where uncertainties are likely to significantly alter the response of the helicopter, an adaptive control strategy should be adopted. Haverdings, Ref(4), has designed one such controller, based on the optimal control of linearized dynamical systems. By modelling the reactions of an 'ideal' pilot, that is one with absolute knowledge of all aircraft states, to changes in flight path demands, a continuous feedback controller was presented. The rotorcraft model used, however, made no provision to alleviate high frequency inputs such as atmospheric turbulence nor were the rotor degrees of freedom modelled. A significant divergence from some of the desired flight states also appeared at the end of the manoeuvre. This suggests that a non-linear controller should be used when simulating manoeuvres using a sophisticated individual blade rotorcraft model.

Difficulty arises in designing a robust and accurate control law using the established parametric techniques (eigenvalue assignment, LQ optimisation) as well as non-parametric frequency domain based techniques (H^{∞}, etc.) as they rely primarily on a feedback loop in the control law. Tischler, Ref(5),has observed that using only the rigid body modes as the measured states for implementation into the main feedback loop may cause the coupled body/rotor modes to become unstable.

This destabilisation of the rotor dynamics has further been explored by Ham, Ref.(6). To alleviate these instabilities, accurate knowledge of the rotor states, flap, lag etc., for inclusion in the feedback loop is essential, so increasing the complexity of the controller. A pilot is, however, able to fly the helicopter along any realistic flight path without having knowledge of the rotor states, adjusting the controls based only upon rigid body dynamic information. The pilot is able to perform this operation by applying the controls not continuously, as in a conventional state feedback control law, but at discrete time intervals. The benefits to be gained, in the form of reduced complexity, from designing a control law based on pilot inputs and responses are therefore evident. It is therefore the aim of this paper to present a simple, heuristically insightful, active control algorithm mimicking pilot inputs which will fly a fully non-linear helicopter mathematical model along a predefined flight path.

2.0 Turbulence model

To demonstrate the disturbance rejection properties of the algorithm, the simulation is flown through an obstruction induced turbulence field. By using a commercial CFD package (FLUENT) the steady state turbulent wake behind any modelled obstacle can be obtained in terms of inertial velocity components at spatial locations. From Ref.(3), the position of each blade element is known and through a series of axes transformations the local aerodynamics can be modified by superimposing the transformed atmospheric velocity onto the local still-air blade element velocity. Similar modifications are made to the fuselage and tailplane aerodynamics. By using each blade element as a sampling station, a cyclostationary representation of the turbulence is afforded. Employing rotational sampling, Ref.(7) enables a more accurate representation of low amplitude, high frequency vibratory forcing, not evident in the conventional body or hub-fixed sampling methods.

Although RASCAL (Rotorcraft Aeromechanic Simulation for Control AnaLysis), Ref(9), operates in 3-D space, a 2-D plane may be used in the construction of the turbulence field, if an appropriate obstacle is chosen, fig(2.1). The atmospheric model, however, remains active in all three dimensions. Even if the obstruction is complex, a general 'first-order' approximation to the solution can be obtained using a fairly simple model. This is shown by the oil-rig approximation, fig(2.2). Two severe operational landscapes were chosen to ensure a realistic test of the algorithm;

1.Flight at low level in close proximity to a tower block and

2. Simulation of the approach to an offshore oil platform.

In scenario 1, the helicopter was required to maintain trim throughout the flight, so illustrating the disturbance rejection properties of the controller, while scenario 2 demanded a flare to hover following a 9° flight path (from an initial flight speed of 10 knots) landing on the flight deck of the oil-rig.

3.0 Rotorcraft Model.

The helicopter mathematical model RASCAL (Rotorcraft Aeromechanic Simulation for Control Analysis) used in the simulation is a fully coupled, individual blade/blade element model. Table 1 highlights the principal features of the model.

Model item	Characteristics
Rotor dynamics (both rotors)	• up to 10 individually-modelled rigid blades • fully-coupled flap, lag and feather motion • blade attachment by offset hinges & springs • lag damper
Rotor loads	• aerodynamic and inertial loads represented by up to 10 elements per blade
Blade aerodynamics	• lookup tables for lift and drag as function of angle-of-attack and Mach number
Wake model	• momentum-derived dynamic wake model • uniform and harmonic components of inflow • rudimentary interaction with tail surfaces • ground effect
Transmission	• coupled rotorspeed and engine dynamics • up to 3 engines • geared or independently-controlled rotor torque
Airframe	• fuselage, tailplane and fin aerodynamics by lookup tables or polynomial functions
Atmosphere	• International Standard Atmosphere • provision for variation of sea-level temperature and pressure

Table (1). Mathematical model description.

4.0 Flight path generator.

The flight path generation model determines the desired states of the aircraft as a function of time. By careful choice of the primary states (states to be controlled) it is possible through the presence of rigid body cross coupling effects to reduce the number of required control states. Inertial positions (position of the aircraft centre of gravity wrt an earth-fixed reference frame) and, if required, inertial velocities, along with heading angle ψ , form the primary state variables used to define the flight path, i.e.

$$\mathbf{y}_{DES} = F^n\{x_{edem}, y_{edem}, z_{edem}, \dot{x}_{edem}, \dot{y}_{edem}, \dot{z}_{edem}, \psi_{dem}, \dot{\psi}_{dem}\}$$

The inertial velocity components are included, where necessary, to provide damping in the primary states induced by the application of the controls. The desired output vector is given,

$$\mathbf{y}_{DES}(t_{k+1}) = \mathbf{y}_{trim}(0) + \mathbf{X}_{des} \cdot t_{k+1}$$

where $\mathbf{y}_{trim}(0)$ contains the trim values of the primary states and $\mathbf{X}_{des}$ is a constant vector of time derivatives. The vector $\mathbf{y}_{des}$ is used as an input to the control algorithm error or 'cost' function.

The form of the vector $\mathbf{X}_{des}$ varies with the simulation objective, i.e., it determines whether a trim is to be maintained or a more severe manoeuvre simulated. Manoeuvres such as the flare to hover, which is presented in this paper, are calculated using a constant deceleration applied to the inertial frame velocity components. Accelerations are chosen such that a constant flight path is maintained throughout. The equations used, appendix(1), are configured such that the helicopter is constrained to fly to a predefined position, along the specified flight path irrespective of the time taken. This induces a large computational cost which can be alleviated by tuning the initial altitude, such that the descent to zero ft (which signifies the end of the manoeuvre) occurs within a specified time.

5.0 Controller.

The control algorithm used on this project was a model following error optimisation routine with a strong predictor/corrector element. The algorithm assumes an ideal observer is modelling the system dynamics, i.e.

$$\hat{\underline{X}} = \underline{X} \qquad \text{Eq}^{n}(5.1)$$

allowing all the states to be used in the construction of the error function.

The discrete output vector can be expressed as a non-linear function of the states and controls.

$$\mathbf{y}(t_k) = F\,(\,\mathbf{x}(t_k)\,,\,\mathbf{u}(t_k)\,) \qquad \text{Eq}^{n}(5.2)$$

If the controls are held constant over the control application interval T and a Zero-Order Hold is employed, then the output at time t_{k+1} is a complex function of the control inputs at t_k.

$$\mathbf{y}(t_{k+1}) = G\,(\,\mathbf{u}(t_k)\,) \qquad \text{Eq}^{n}(5.3)$$

The desired output vector, $Y_{DES}(t_{k+1})$, obtained from the flight path generation model, enables definition of an error matrix,

$$E(\mathbf{u}(t_k)) = \mathbf{y}(\,t_{k+1}\,) - \mathbf{y}_{DES}(\,t_{k+1}\,) \qquad \text{Eq}^{n}(5.4.1)$$

or, from Eq^{n}(5.4)

$$E(\mathbf{u}(t_k)) = G\,(\,\mathbf{u}(t_k)\,) - \mathbf{y}_{DES}(\,t_{k+1}\,) \qquad \text{Eq}^{n}(5.4.2)$$

The control deflections required to minimise Eq^{n}(5.5.2) are found using a Newton-Raphson iteration.

$$\mathbf{u}_{i+1}(t_k) = \mathbf{u}_i(t_k) - (J[G\,(\,\mathbf{u}(t_k)\,])^{-1}\,E(\mathbf{u}_i(t_k)) \qquad \text{Eq}^{n}(5,5)$$

where i is the iteration index and J[] is the jacobian,

$$J\big|_{i,j} = \left[\partial E_i\left(u(t_k)\right)/\partial u_j\left(t_k\right)\right] \qquad \text{Eq}^{n}(5.6)$$

The iteration loop is terminated when $E(\mathbf{u}(t_k))$ falls below a pre-set tolerance. The control deflections predicted by the algorithm are then fed back as inputs to the actual system and the process continues for the next time interval. A flow diagram of the control algorithm is shown in chart(1).

6.0 Results.

6.1 Disturbance Rejection

To illustrate the disturbance rejection properties of the algorithm a single main and tail rotor helicopter, the Puma, was constrained to fly at close proximity to a tower block, operational landscape 1, illustrated in figure(2.1). The c.g. of the helicopter was positioned 40 metres to the right of the east facing wall. A trim airspeed of 10 knots was chosen to ensure that the vehicle dynamics were affected over a wide bandwidth, Ref.(3). The integration time interval, expressed in terms of the azimuthal displacement of the tail rotor, was 45° (0.00569 sec), with a control application interval, T, of 8 complete tail rotor turns (0.365 sec).

Fig(6.1.1) shows the motion of the uncontrolled versus controlled aircraft in the gust. After only 9 seconds, a lateral drift of almost 35 metres is present, along with a reduction in altitude of 3 metres in the free response. This motion is indicative of a 'spiral dive' type of rigid body divergence, a dangerous flight state especially at low level in close proximity to a building. Activating the controller (with reference to the flight states) results in a maximum lateral deviation from trim of less than 0.002m. Similarly, there is a significant reduction in the maximum altitude change. The overall effect is to maintain a flight path of $\gamma = 0°$, as illustrated by comparison of figs(6.1.2) and(6.1.3).

From Ref.(3), flying through atmospheric turbulence induces an additional vibratory component to the rotor loading. Fig(6.1.4) shows time histories of the uncontrolled aircraft body accelerations. The vibratory component is small compared to the low frequency (rigid-body) accelerations, which are excited due to the 'ordered' nature of the turbulence field. Fig(6.1.5) shows the time histories of the body accelerations with the control algorithm activated. The large amplitude, low frequency component has been eliminated from each body axis acceleration, as required.

6.2 Simulation of Manoeuvres

This section of the report deals with the simulation of a relatively gentle helicopter manoeuvre performed initially in still air. The manoeuvre is a flare to hover, following a pre-determined glide path, described solely in terms of a linear

deceleration of the longitudinal (x,z) inertial velocity components. The same helicopter configuration as in the disturbance rejection section was used.

The necessary retardation was calculated using basic Newtonian mechanics. Initially a target point was set relative to the starting trim position in the inertial frame. Boundary conditions of zero inertial velocity at the manoeuvre termination point were also imposed. The equations used to calculate the required deceleration, manoeuvre time and demanded inertial positions and velocities are given in appendix(1).

The first case consisted of a 25 knot flight along a 9° glide slope. The initial altitude was tuned to 66 ft, giving a manoeuvre time of 20 seconds. From fig(6.2.1) it is apparent that the helicopter tracks the demanded flight path very well. On the scale shown there is no significant error developing, even after the helicopter comes to rest (in an inertial velocity sense) i.e. as the algorithm attempts to trim the helicopter at hover. For such a delicate flight state as the hover, finding the controls required to trim the aircraft may be better accomplished when using this method if information is available for the body attitudes and rates as well as the constraints. This accounts for the sudden instabilities developing in the lateral/directional motion after 20 seconds of simulation, fig(6.2.2).

Fig(6.2.3) shows the control displacements required to perform this manoeuvre. As with disturbance rejection, a zero-order hold is assumed and the calculated control perturbations applied as step inputs. As expected, as the aircraft pitches nose up, a steady increase in collective main rotor pitch is applied. The tailrotor collective also increases due to the presence of a strong coupling between the roll/pitch/yaw dynamics. Fig(6.2.4) is a plot of the lateral vs. longitudinal cyclic pitch of the main rotor and gives an indication of the stick movement required to perform the manoeuvre (this is an approximate representation as no actuator dynamics were modelled).

In the second flare an initial flight speed of 40 knots was used, again with a 9° glide slope. This corresponds to a velocity of approximately $5ms^{-1}$ in the body axis z-direction. The uniform component of inflow velocity in this trim state is given by RASCAL to be approximately $6ms^{-1}$. As the incidence of the rotor disc changes during the manoeuvre, changes in the inflow velocity occur. If the inflow and rate of descent match there will be no net flow through the rotor, leading to a numerical instability developing within the model. This condition therefore represents almost a

'worst case' scenario for the algorithm to deal with. Indeed, it proved necessary to include weighted velocity error terms ($\dot{x}_e$ - $\dot{x}_{edem}$) etc. in the controller error vector, $E(\mathbf{u}(t_k))$, to ensure that the convergence criteria would be met.

From fig(6.2.5), it is apparent that the controller managed capably to perform the manoeuvre. As with the 25 knot case, there is little residual error build up in either the x_e or z_e displacements. The lateral displacement and heading errors are also well within acceptable boundaries, Fig(6.2.6). However, due to the increased severity of the manoeuvre there has been a dramatic increase on both the overall amplitude and vibratory component of the body accelerations, Fig(6.2.7). These accelerations far exceed existing ride quality criteria and would therefore have to be reduced in an actual helicopter control system by an inner loop ride quality controller.

6.2.1 Constraint Oscillations.

Considering a second order dynamic system, a constant input will result in an oscillatory response which can be characterised in terms of frequency of oscillation and asymptotic damping. If the output, or response, must be constant, then it is conceivable to assume that an oscillatory input will be required. Thomson, Ref.(8), has discovered that by applying constraints, i.e. demanding a constant output, an oscillatory response is introduced to the secondary, or indirectly influenced states. From the standard 6 dof., 9 state linear representation of the helicopter, the primary variables or those states heavily influenced by the constraints are u, v, w & r, while the unconstrained states are p, q, θ, ϕ. The 9^{th} state, ψ, is used as one of the constraints. From Ref.(8), the frequency of the constraint oscillations can be predicted, (Fig(6.2.8) shows these oscillations present in p, q, θ, ϕ for the 10 knot manoeuvre). For the 10 knot trim case, the damped frequency of oscillation for the roll mode was calculated as $w_{d_{(1)}}$ = 0.4909 Hz and the pitch mode as $w_{d_{(2)}}$ = 0.3183 Hz. These frequencies may be observed in the time histories of Fig(6.2.8). Figs(6.2.9-6.2.12) show the zero mean power spectral density curves for the secondary states over a range of sampling intervals. The effect of the time interval between control applications is evident in the frequency shifts shown around the predicted oscillation frequencies. It is therefore reasonable to assume that the oscillations present in the secondary variables occur due to the constraints imposed on the flight path variables, as predicted by Thomson, Ref(8).

6.3 Effect of Control Algorithm Parameter Changes

6.3.1 Tolerance limit

Consider Fig(6.3.1). These results were obtained using the 10 knot flight speed case and by setting a tolerance limit of tol = 0.0001 on the inertial co-ordinate and tol/10 on the heading angle variables contained within the control algorithm error vector (see chart(1)). By observing the output from the controller it was apparent that there was a build up of residual errors in the lateral position constraint, y_e, leading primarily to greater demanded lateral cyclic displacement. Reducing the tolerance on y_e by two orders of magnitude prevented large errors from occurring, enabling the aircraft to follow the demanded flight path more accurately, Fig(6.3.2). The amplitude of constraint oscillations was also reduced (compare fig(6.2.8) with fig(6.3.3)) along with the required control deflections, fig(6.3.4). As small control deflections are desired (improved efficiency of the controller) tuning of the tolerance limits can be seen to improve the performance of the algorithm. For the more severe manoeuvres (25 and 40 knot cases etc.) tolerance modification acts to aid convergence of the controller rather than explicitly reduce the amplitude of the constraint oscillations.

6.3.2 Significance of the Control Application Interval.

This next section will explore the effects of altering the control application interval on the performance of the control algorithm. The 10 knot trim in still air was chosen, using both position and weighted velocity terms in the cost function. 4, 6, 8, 10 and 12 turns of the tailrotor were chosen, corresponding to times of 0,188s, 0.282s, 0.37s, 0.47s and 0.56s between successive control inputs. At T = 4 turns, a high frequency oscillation is present caused by the influence of the rotor dynamics on the controller. From fig(6.2.9), it can be seen that perhaps the first regressive flap mode is evident (≈1.5Hz) along with the rotor coning mode at about 4Hz. At T = 12 turns rigid body modes begin to develop, consequently their effects are included in the controller. So that an overall comparison can be performed, define the Cumulative Standard Deviation coefficient by

$$CSTD = \sum_{i=1}^{n} STD_i$$

where $STD = [\, y_e, z_e, \theta, \phi, \psi, u, v, w, p, q, r, \dot{u}, \dot{v}, \dot{w}\ \theta_o, \theta_{1s}, \theta_{1c}, \theta_{tr}]^T$

Table(2) contains the cumulative standard deviation coefficients as a function of the control application interval.

Nº of turns	4	6	8	10	12
CSTD	1.1669	0.3486	0.2273	0.3112	1.3909

Table (2)

The results in Table (2) suggest that there is an optimum control application interval at approximately 8 turns of the tailrotor. This information, in conjunction with the practice of tuning the tolerances should improve the overall performance of the algorithm. It should be noted that control application intervals corresponding to 2 and 16 turns of the tailrotor caused the algorithm to fail. This suggests that in addition to an optimum time interval T, there exists a finite band of admissible application intervals, outside of which the algorithm will fail. This statement is further elucidated by fig(6.3.5). This effect may be due, in part, to the natural dynamics of the helicopter. A small control interval (T < 4 turns) leaves little time for the effects of a control perturbation to be felt by the error vector (the section of the controller performed by GENISA). This leads to an ill-conditioned jacobian matrix which may lead to the build up of numerical instabilities in the controller. By setting the control interval too great (T > 12 turns), the natural rigid body dynamic modes of the system develop increasing the magnitude of the elements in the error vector, possibly resulting in a convergence failure. This also leads to large control deflections which may result in a control authority exceedence failure.

6.4 Oil Rig Landing.

The simulation of a landing flare aimed at the platforms' helideck in a turbulent scenario was used as the final test of the algorithm. The algorithm is required to perform well in both the manoeuvring and disturbance rejection roles. The turbulence field used was that designated scenario 2, fig(2.2), oil rig field. The manoeuvre itself covers what would be the final stage of a standard 9° approach. The initial flight speed was 10 knots with a manoeuvre time of 15 seconds. From the results of section 6.3, the control application interval chosen corresponded to 8 tailrotor turns.

A time response of the longitudinal inertial components is given in fig(6.4.1), showing, as before, that the algorithm tracks the desired flight path well. The

lateral/directional constrained component errors are minimised well, although greater instantaneous lateral drift is observed, fig(6.4.2). A control authority bandwidth comparable to the 25 knot manoeuvre is observed, fig(6.4.3), showing no control limits were exceeded. Overall, the control algorithm performs well with the combined manoeuvre simulation / disturbance rejection demands.

Conclusions.

- A simple control algorithm has been designed which will allow the simulation of helicopter manoeuvres to be performed using an individual blade/blade element rotorcraft model.
- The use of this controller in a turbulence rejection role has been demonstrated and proved to be highly effective.
- The oscillatory motion apparent in the secondary variables is due to the application of constraints on the flight path states.
- The performance of the control algorithm may be significantly enhanced by careful tuning of the error vector tolerance limits
- Stability boundaries for the controller exist and appear to be a function of the sampling interval, T.
- The algorithm performs well in a combined manoeuvre simulation - disturbance rejection role.

Acknowledgements

The authors wish to acknowledge the support of this research by the Defence Research Agency, Bedford.

References.

1 Hess,R.A., Gao,C. *Inverse Simulation of Large Amplitude Aircraft Manoeuvres*, Journal of Guidance, Control and Dynamics, Vol. 16, No.4,1993

2 Rutherford,S. and Thomson,D.G., *Development of a Generic Inverse Simulation Algorithm*, University of Glasgow, Department of Aerospace Engineering, Internal Report No. 9410, July 1994

3 S.S.Houston, R.A.Hamilton,'*Modelling, Simulation and Characterisation of Helicopter Response to Atmospheric Turbulence*', 19th European rotorcraft forum,Paper G18, September 1993.

4 H.Haverdings,*A Control Model for Manoeuvering Flight for Application to a Computer-Flight-Testing Program.*,Vertica Vol.7, No3,pp. 259-269, 1983.

5 M.B.Tischler,*System identification requirements for High- Bandwidth Rotorcraft Flight Control System Design*, Journal of Guidance and Control,Vol13,No5,pp. 835-841,1990

6 N.D.Ham,*Helicopter Individual-Blade-Control Reasearch at MIT 1977-1985*, Vertica, Vol 11, No.1/2,pp. 109-122, 1987

7 G.H.Gaonkar et.al., *Atmospheric Turbulence Simulation for Rotorcraft Applications,* Journal of the American Helicopter Soc., Jan 1993, pp. 84-88.

8 Thomson,D.G. and Bradley,R., *Prediction of the Dynamic Characteristics of Helicopters in Constrained Flight*, The Aeronautical Journal, December 1990.

9 S.Houston, *Rotorcraft Aeromechanics Simulation for Control Analysis - Mathematical Model Description.* University of Glasgow Dept. of Aerospace EngineeringInternal Report No.9123(1991)

Appendix (1) Derivation of the FPG model manoeuvre equations.

The manoeuvre equations in the flight path generation model are derived using simple Newtonian kinematics in conjunction with pertinent boundary conditions. For the flare to hover, two primary boundary conditions are imposed, firstly that a constant flight path angle be maintained throughout the manoeuvre and secondly that the manoeuvre has to terminate when the altitude of the helicopter reaches zero. It is also necessary to define the manoeuvre time, t_m, which, once set, allows calculation of the required accelerations in the longitudinal inertial reference frame, i.e.

$$a_x(t) = \frac{-u_x}{t_m} \qquad \text{Eqn(A1)}$$

$$a_z(t) = \frac{-u_z}{t_m} \qquad \text{Eqn(A2)}$$

Once the accelerations are known, the tuned starting altitude is given by,

$$s_z = \frac{-u_z^2}{2a_z} \qquad \text{Eqn(A3)}$$

A similar operation is performed in the x-direction. The demanded positions and velocities at time t_{k+1} for use in the control algorithm are given by,

$$x_{dem} = u_x t_{k+1} + \frac{1}{2} a_x t_{k+1}^2 \qquad \text{Eqn(A4)}$$

$$z_{dem} = u_z t_{k+1} + \frac{1}{2} a_z t_{k+1}^2 \qquad \text{Eqn(A5)}$$

$$\dot{x}_{dem} = u_x + a_x t_{k+1} \qquad \text{Eqn(A6)}$$

$$\dot{z}_{dem} = u_z + a_z t_{k+1} \qquad \text{Eqn(A7)}$$

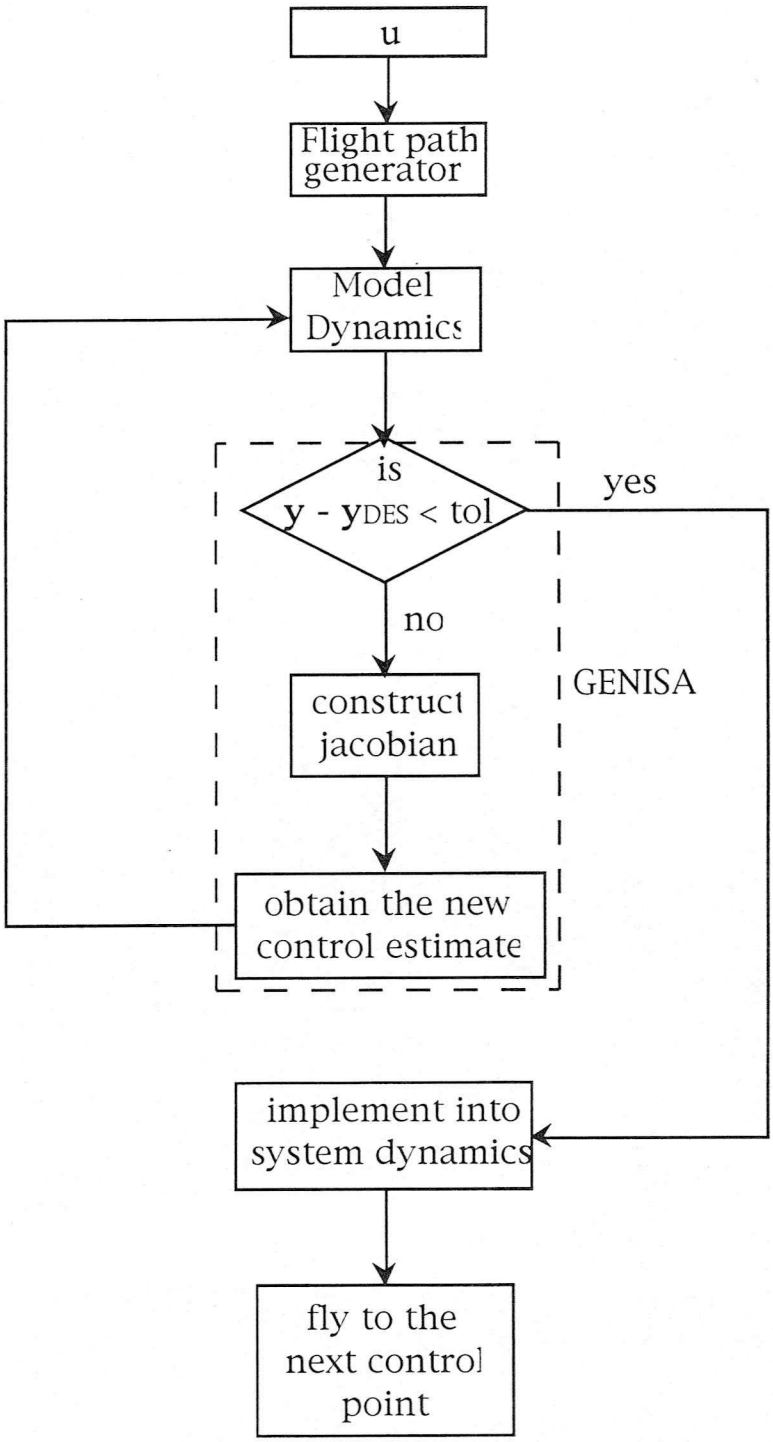

Chart 1. Structure of the control algorithm.

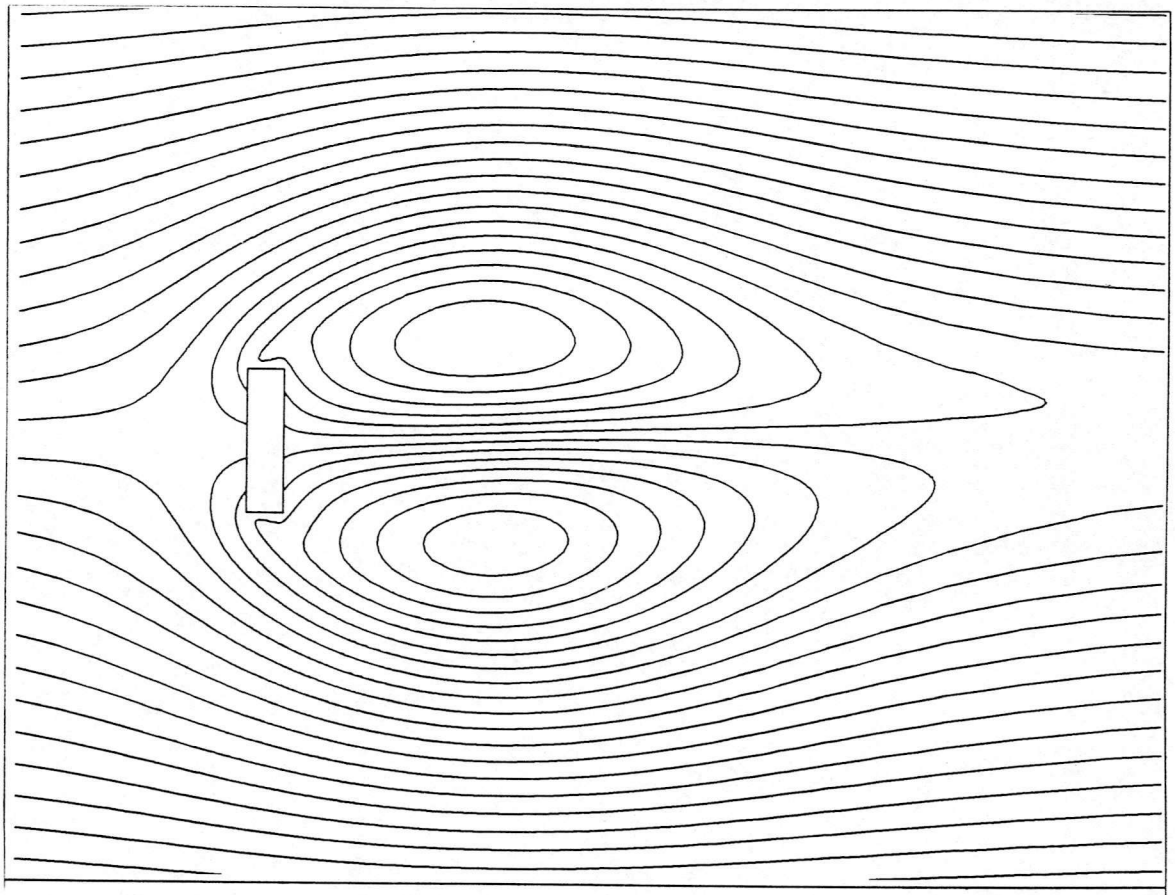

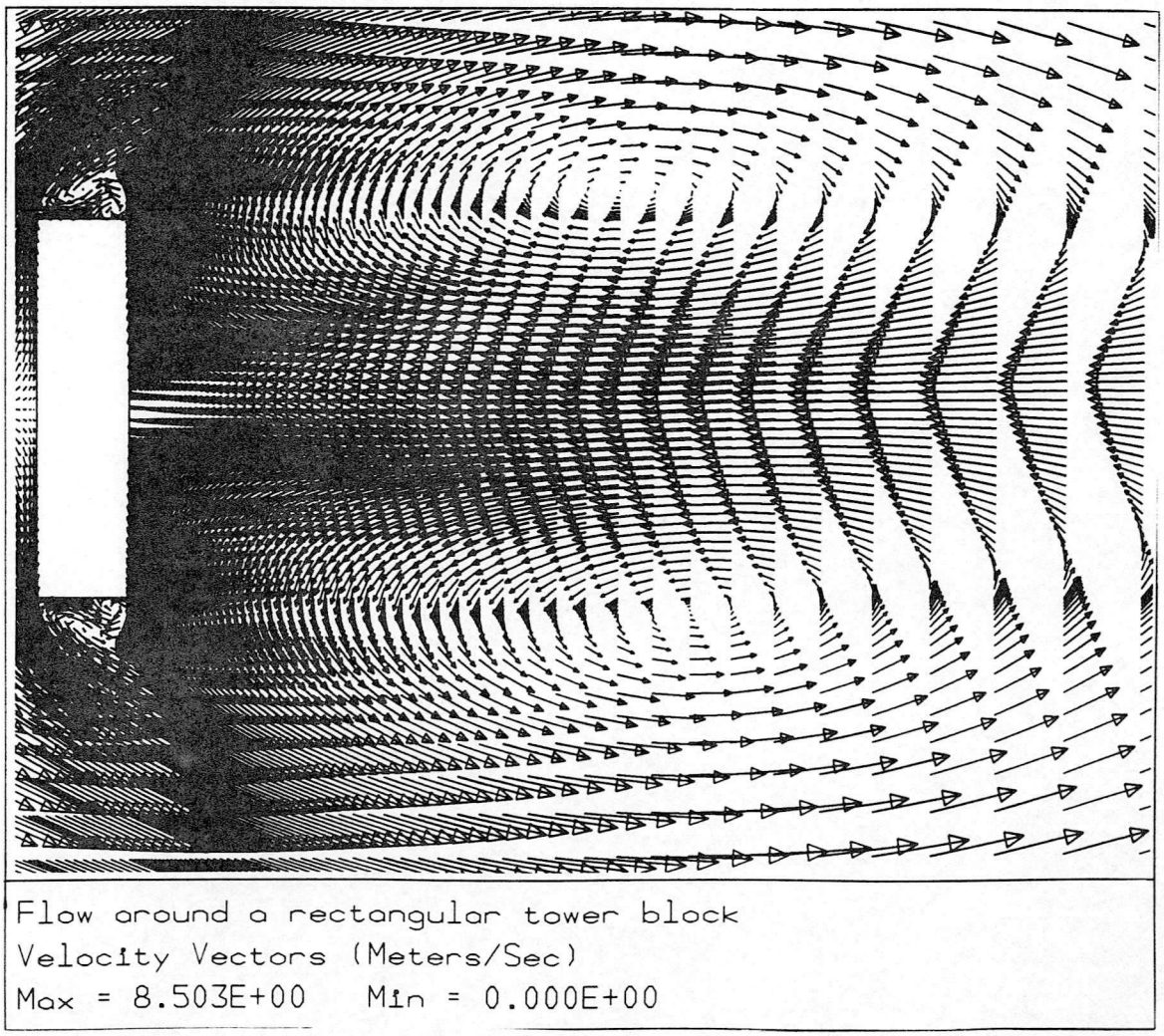

Fig (2.1), Illustration of the flow pattern evolved when passing a rectangular tower block at 2.5 ms^{-1}.

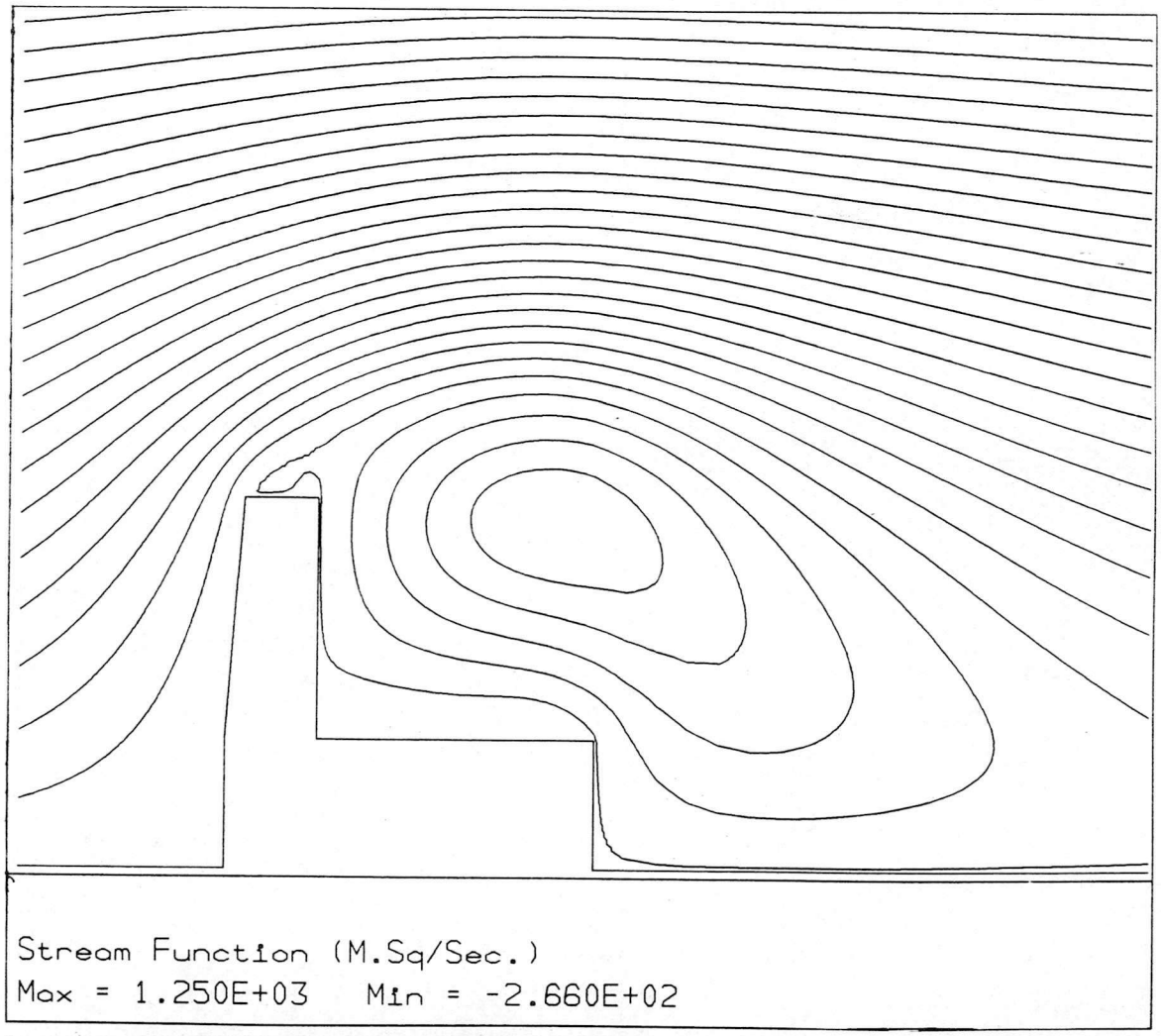

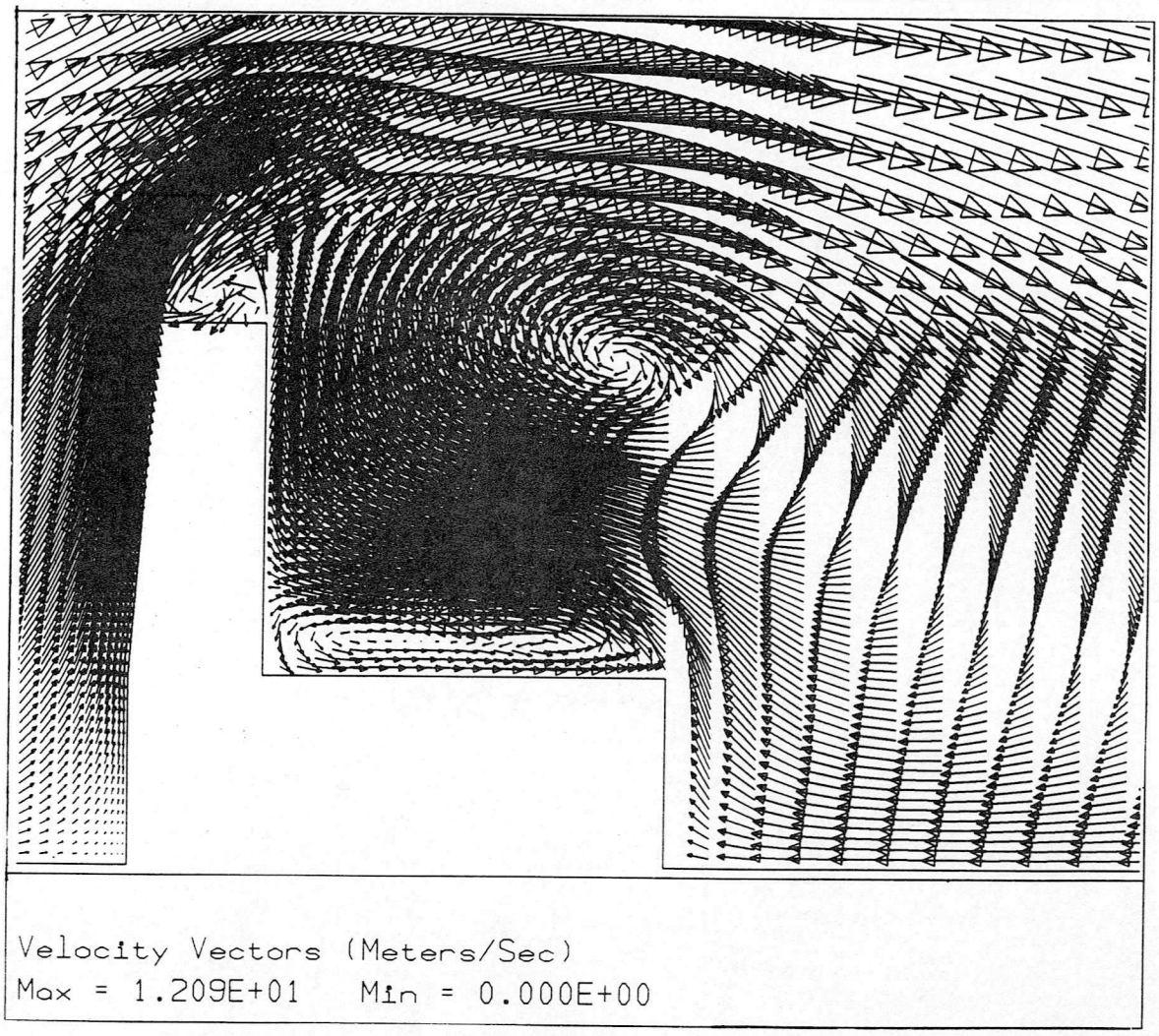

Fig(2.2), Simple representation of the flow pattern induced by an offshore oil platform in a $5ms^{-1}$ freestream.

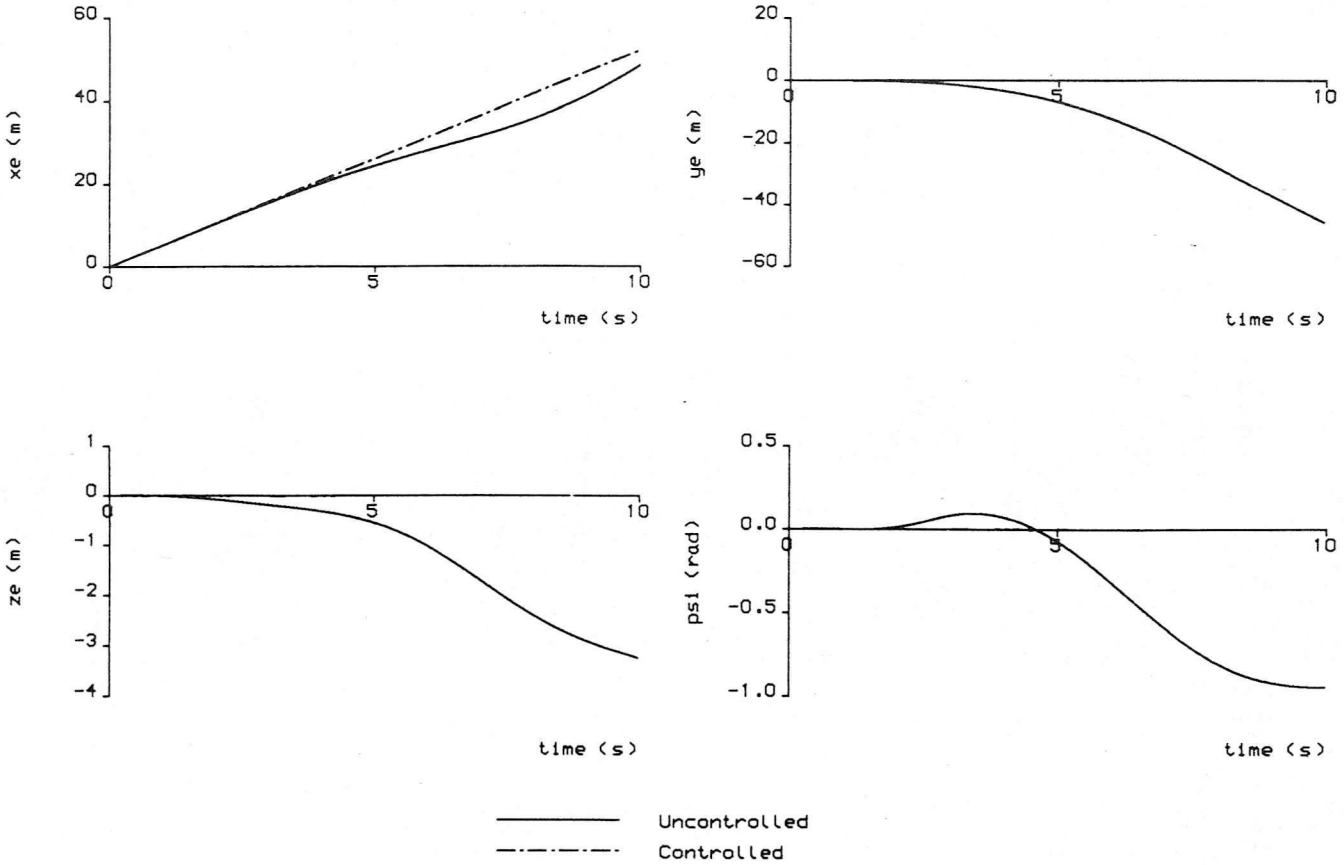

Fig(6.1.1), Uncontrolled vs. controlled puma in operational landscape #1.

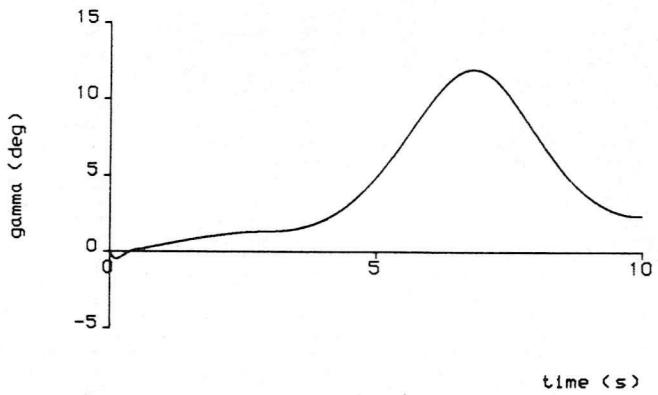

Fig(6.1.2), Flight path angle for the uncontrolled aircraft.

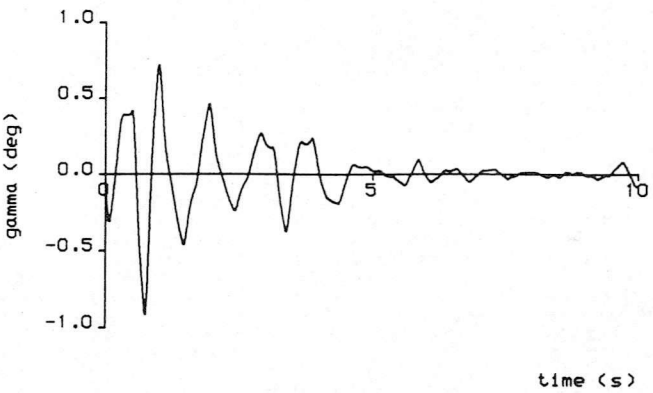

Fig(6.1.3), Flight path angle with controller implemented.

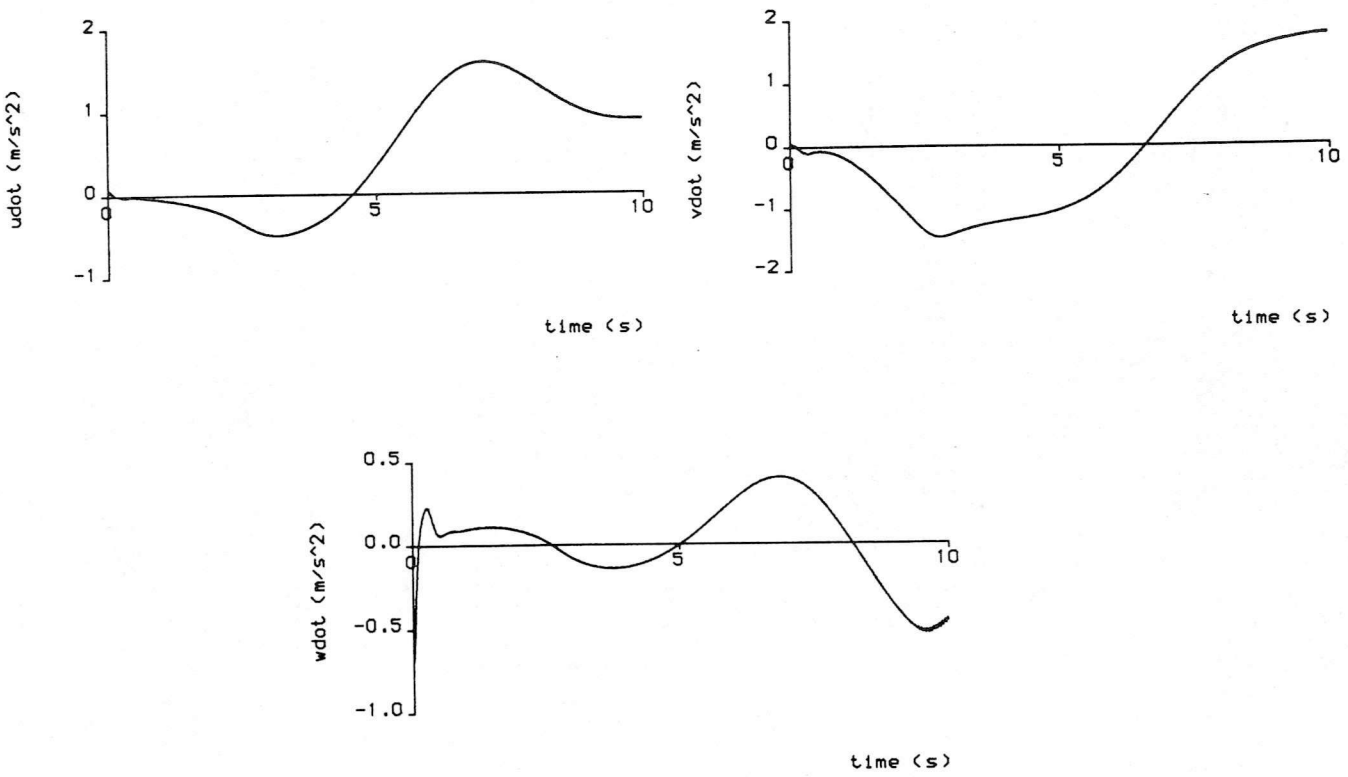

Fig(6.1.4), Uncontrolled turbulence-induced body accelerations.

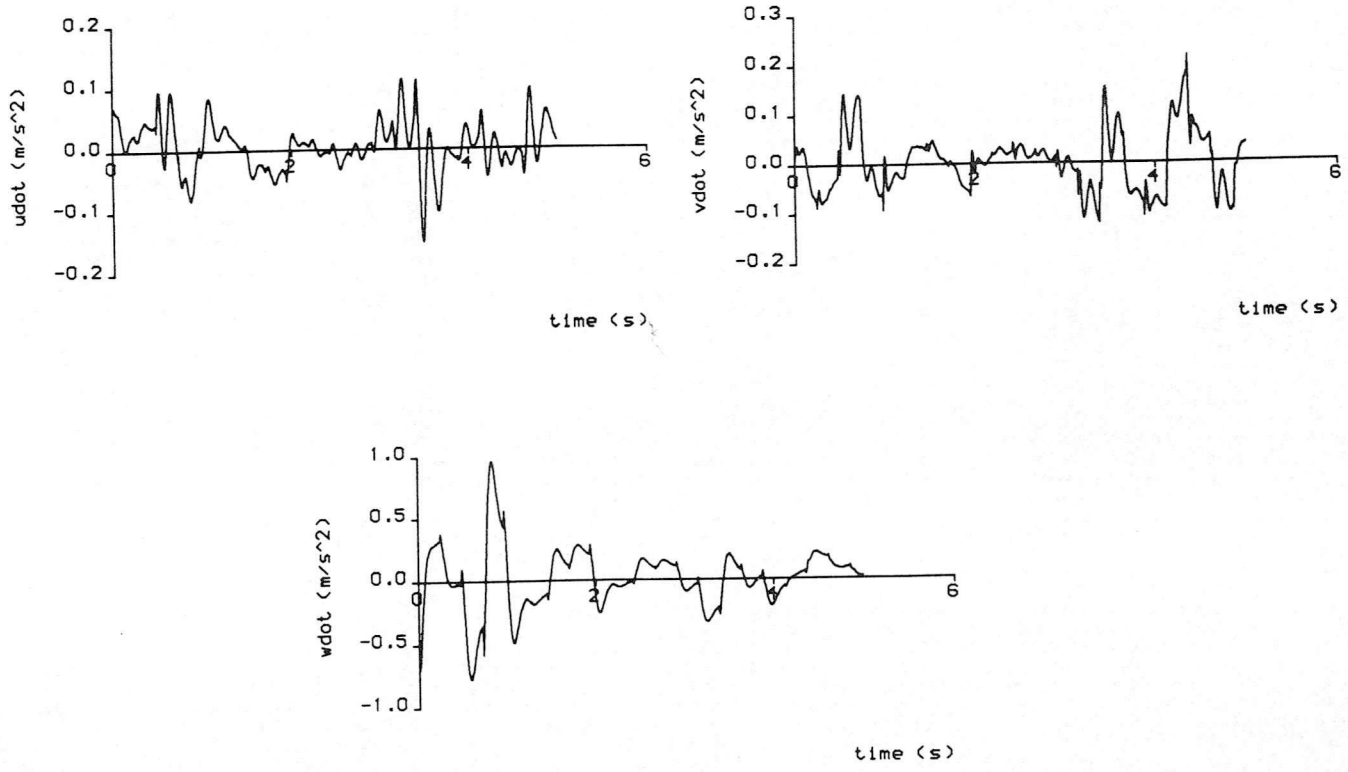

Fig(6.1.5), Turbulence-induced body accelerations with control applied.

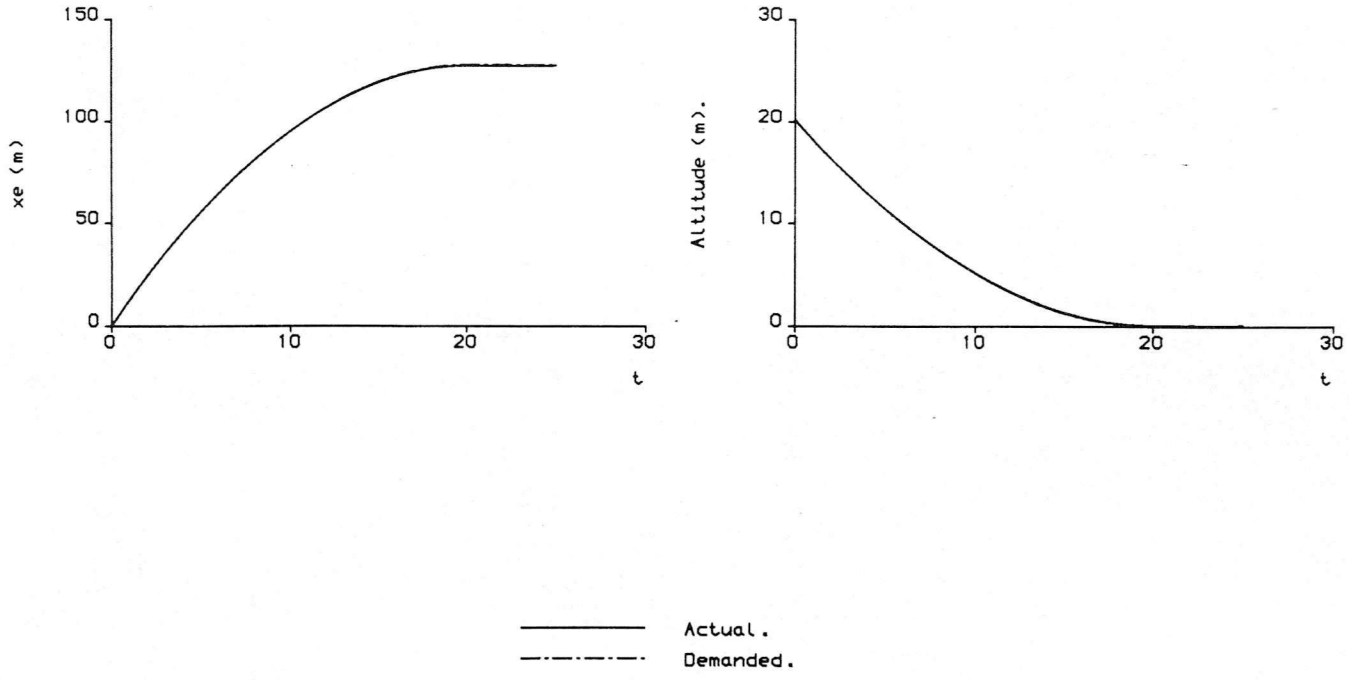

Fig(6.2.1), Controller tracking effectiveness for a 25 knot flare-to-hover.

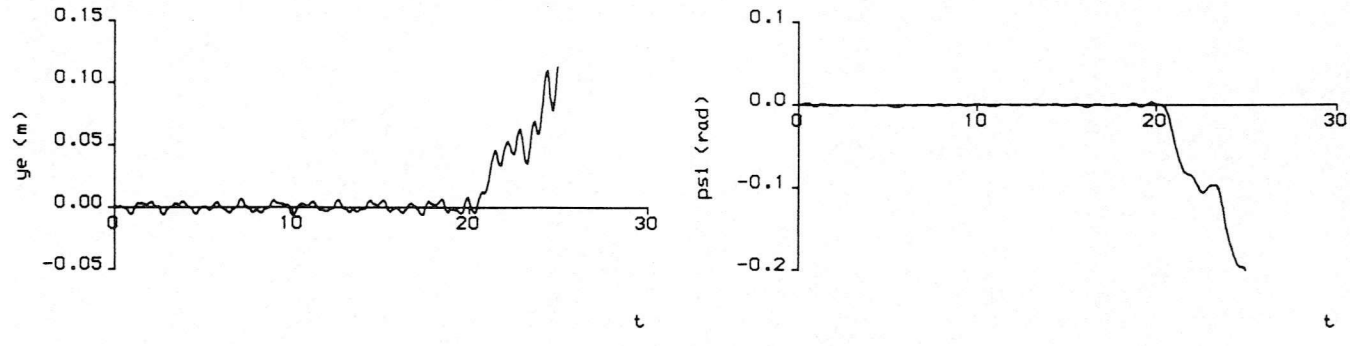

Fig(6.2.2), 25 knot flare-to-hover lateral/directional motion.

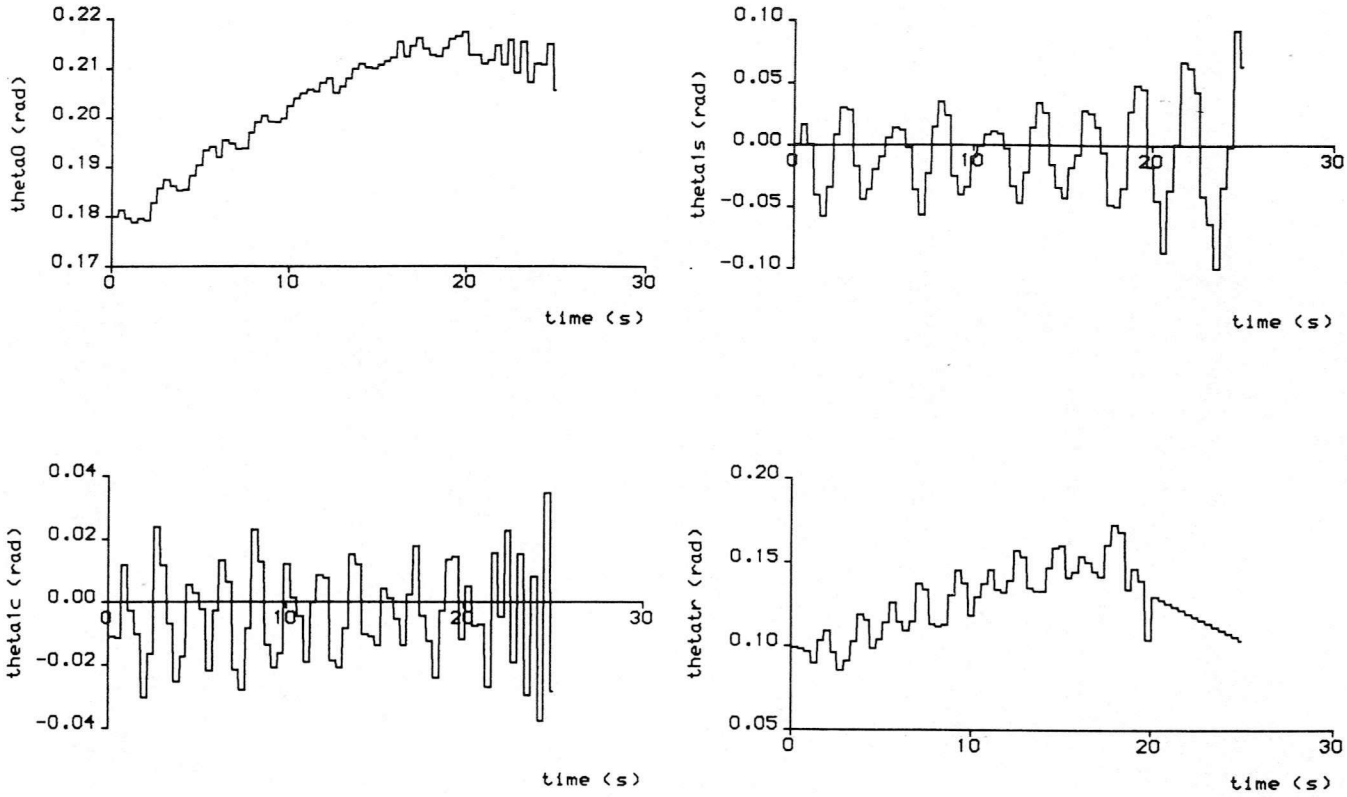

Fig(6.2.3), Control inputs required for the 25 knot flare.

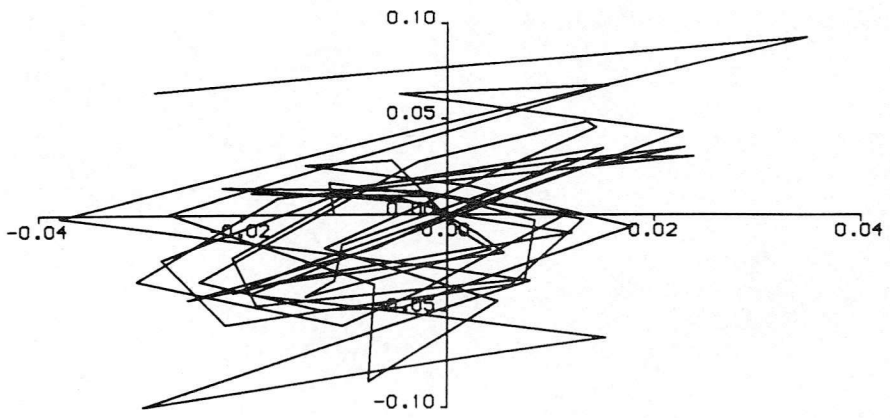

Fig(6.2.4), Main rotor cyclic stick motion, 25 knots.

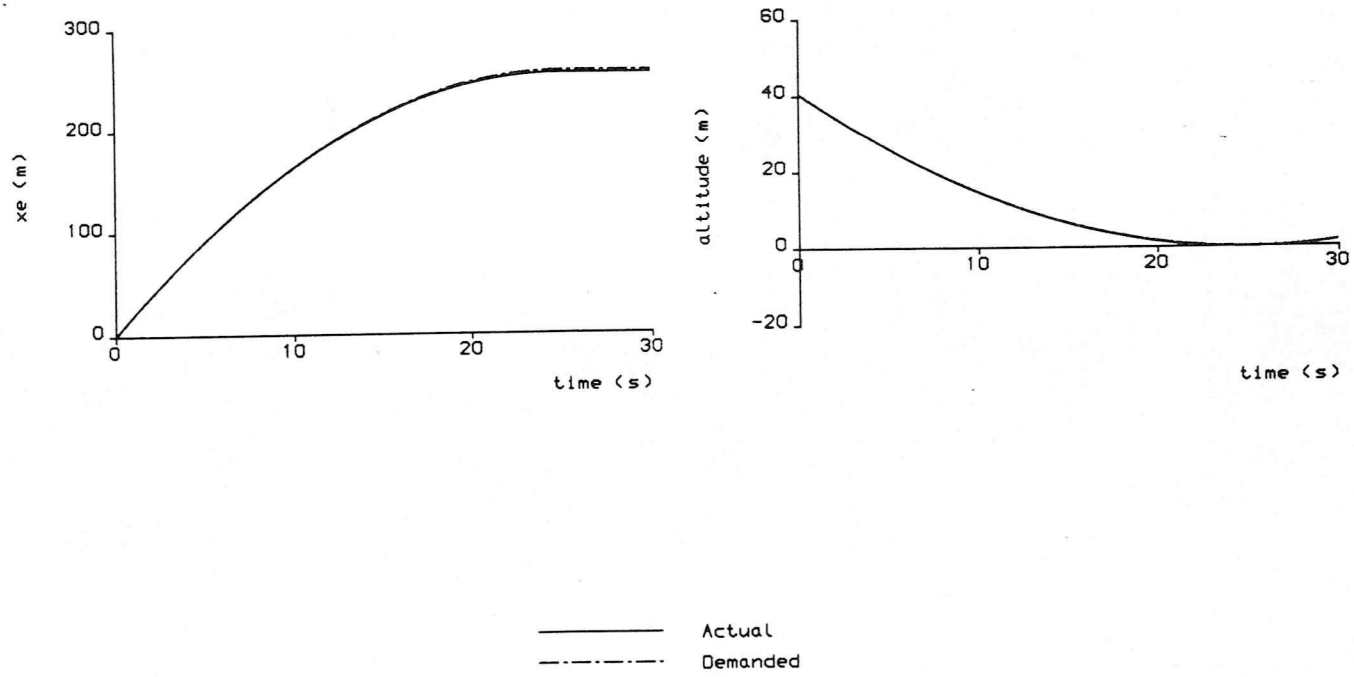

Fig(6.2.5), Control tracking effectiveness for a 40 knot flare-to-hover.

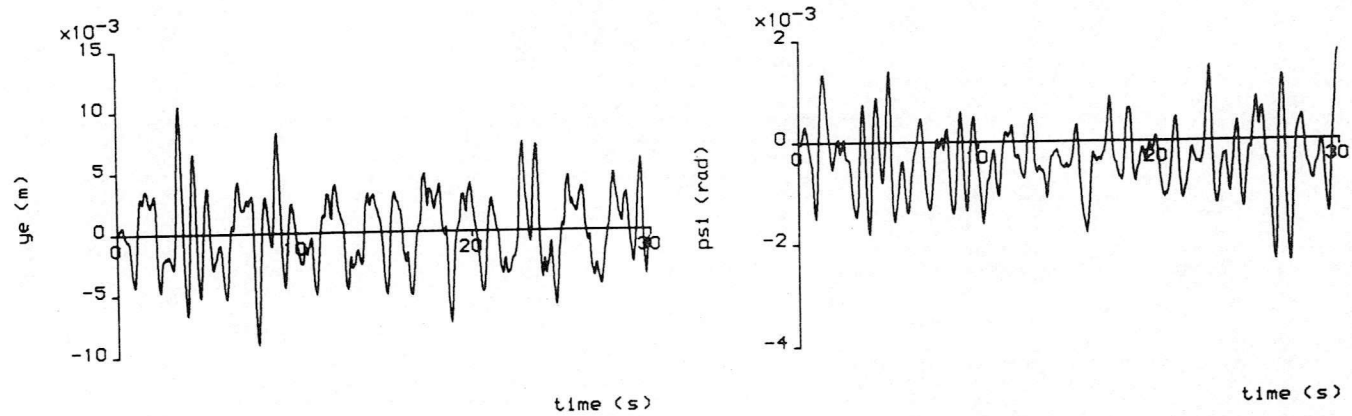

Fig(6.2.6), Lateral/directional motion, 40 knot flare-to-hover.

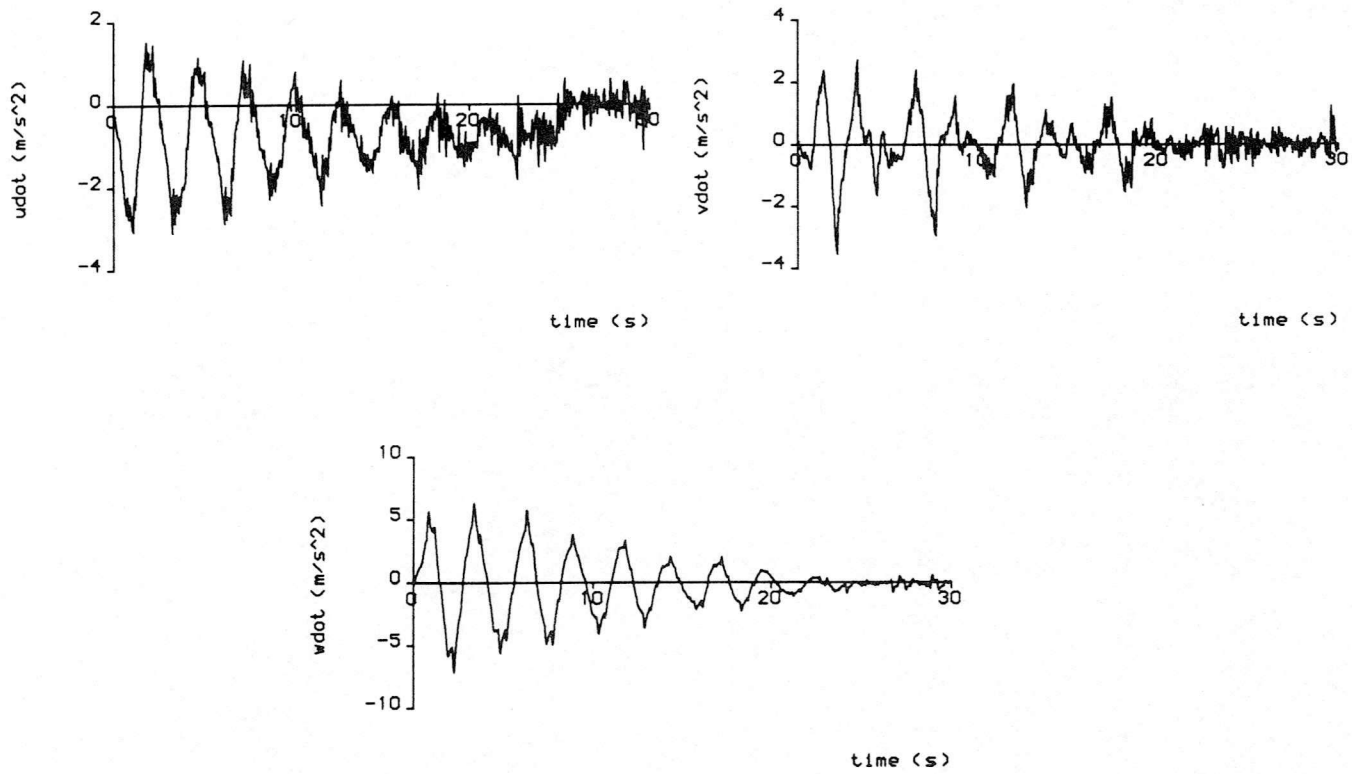

Fig(6.2.7), Body accelerations, 40 knot case.

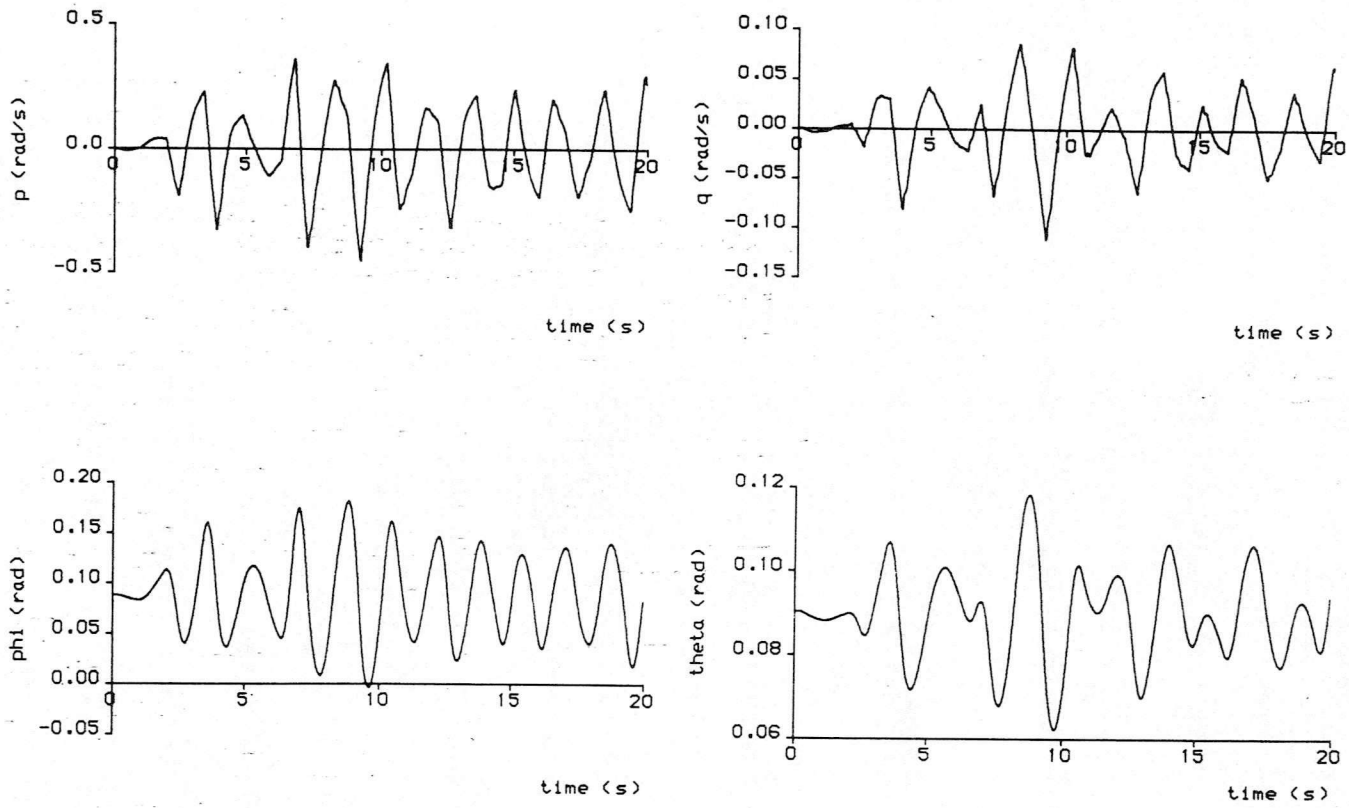

Fig(6.2.8), Constraint oscillations induced by maintaining a 10 knot trim.

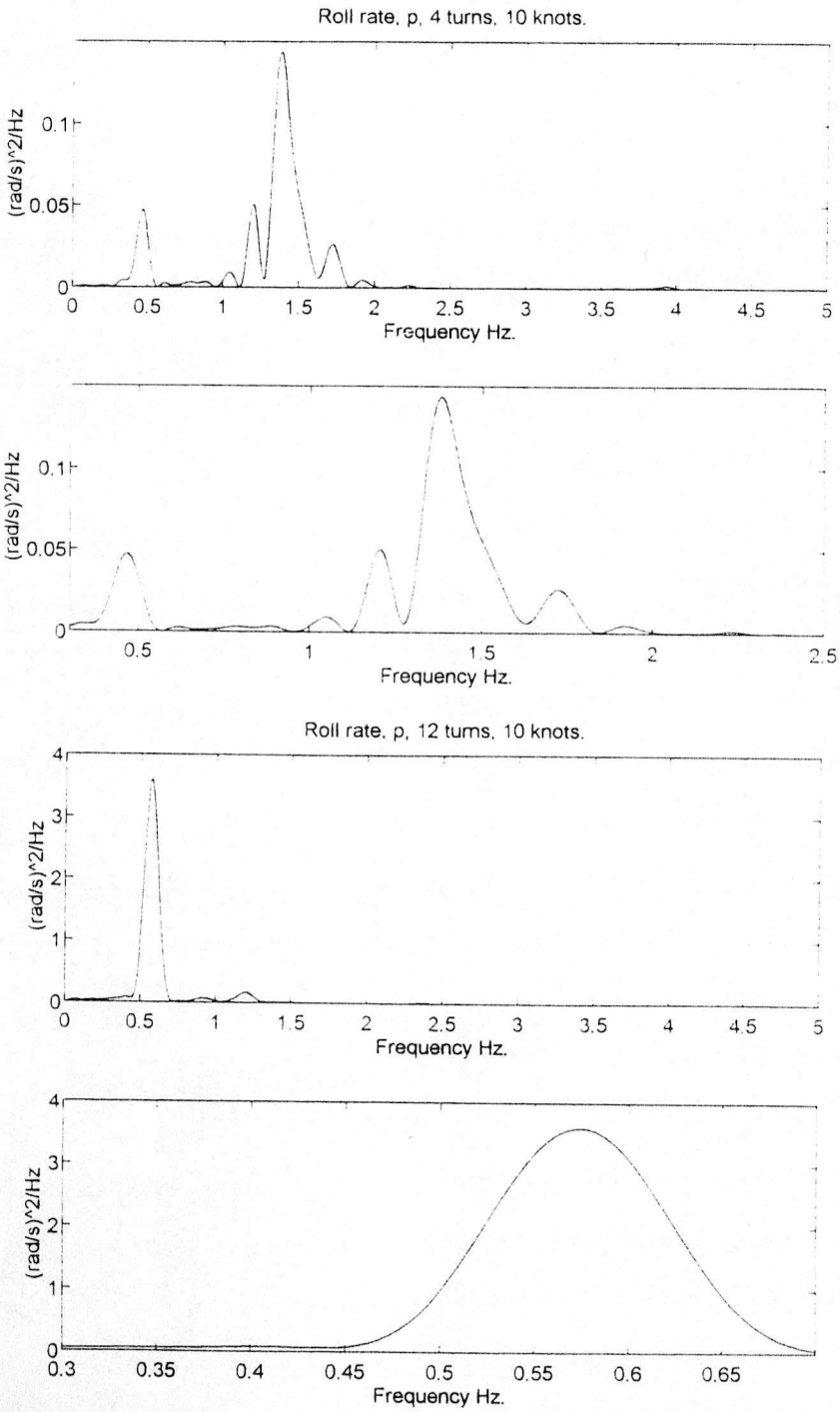

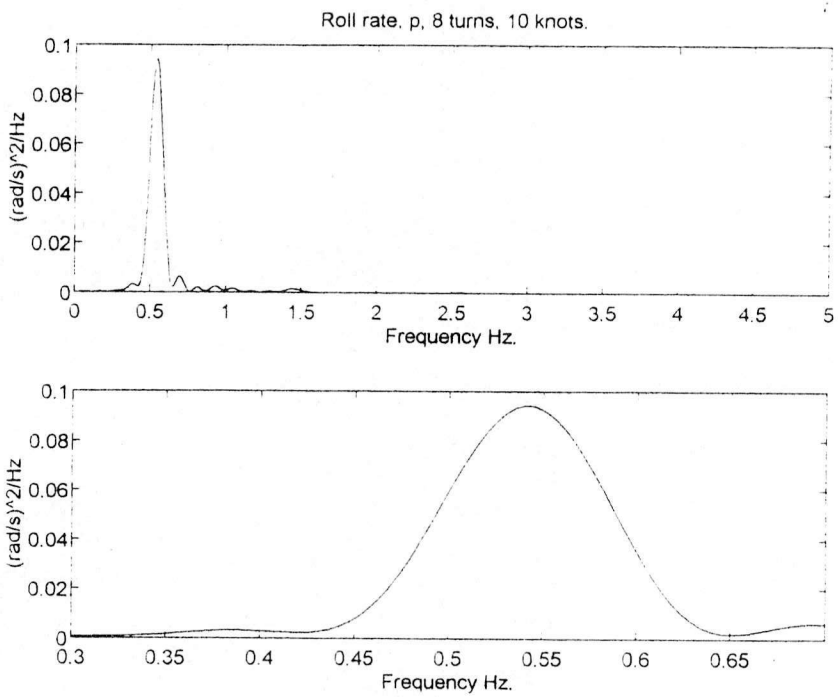

Fig(6.2.9), PSD curves of roll rate, p, 10 knots.

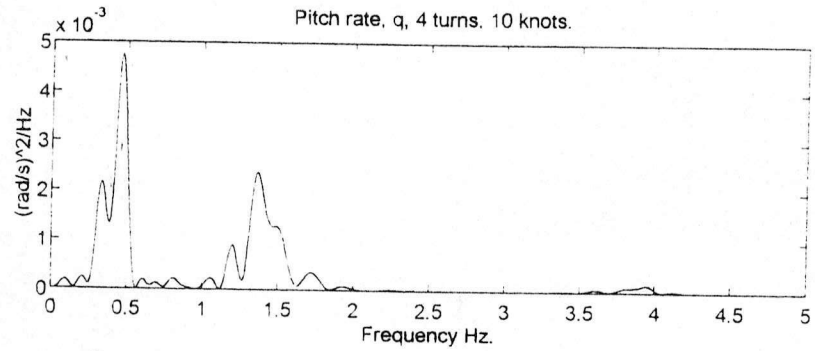

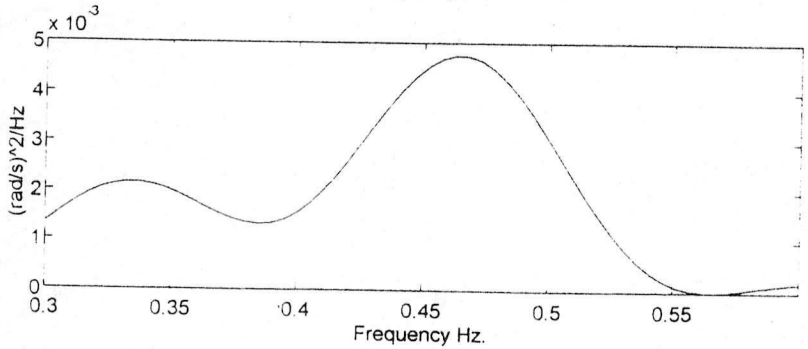

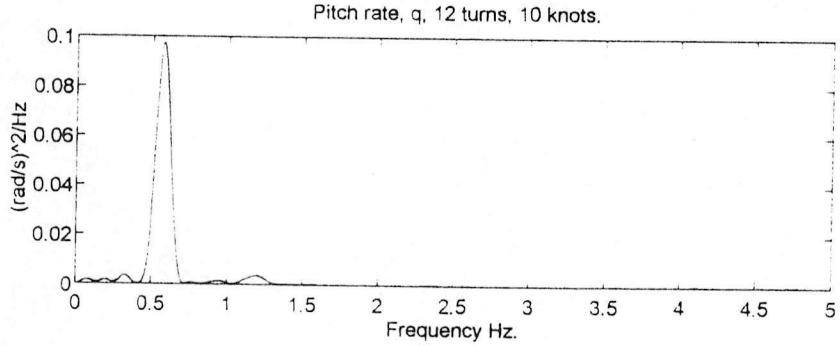

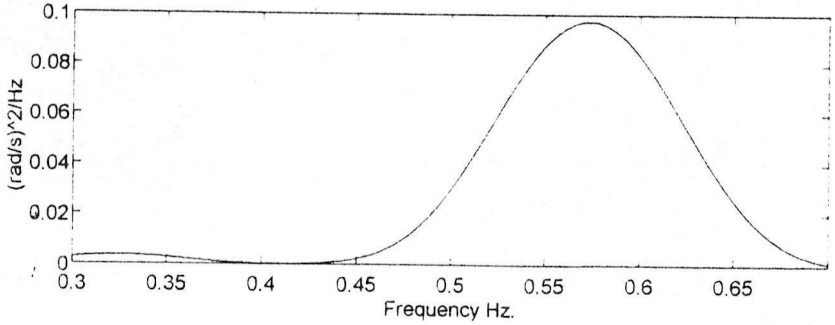

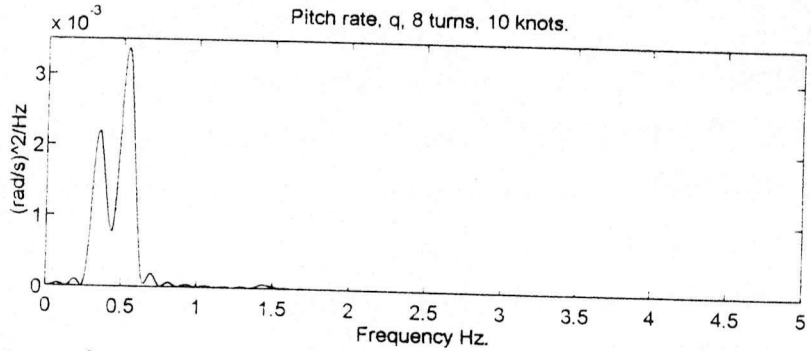

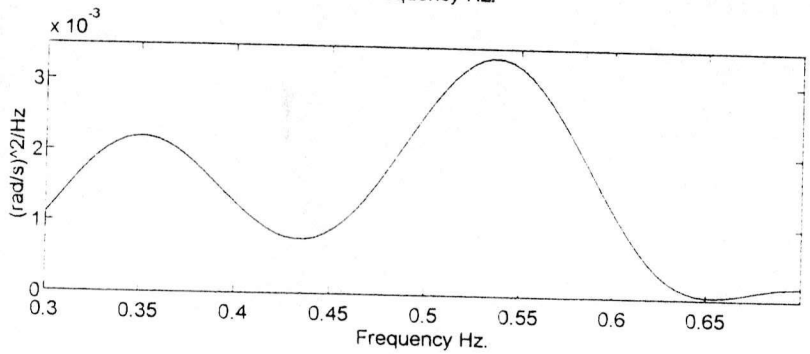

Fig(6.2.10), PSD curves of pitch rate, q, 10 knots.

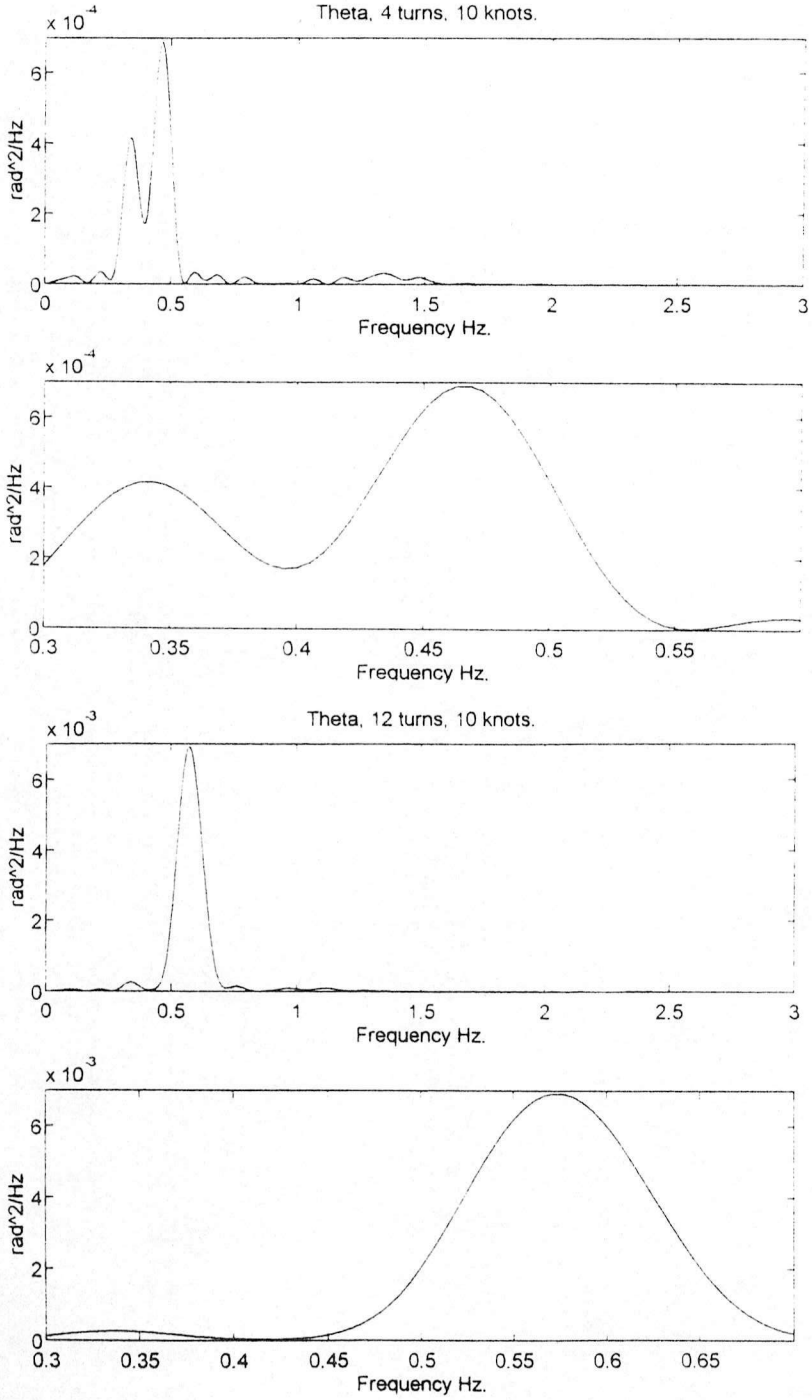

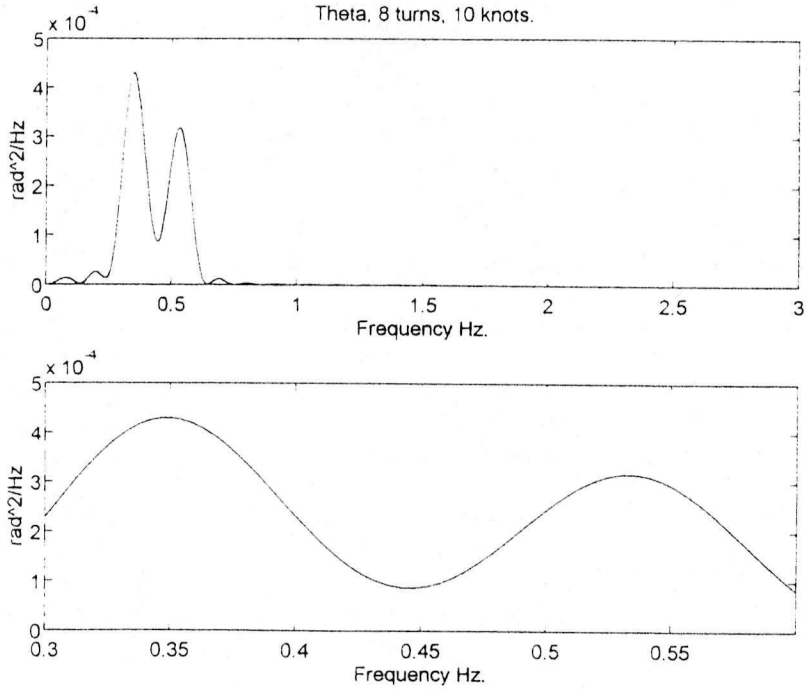

Fig(6.2.11), PSD curves of pitch angle, θ, 10 knots.

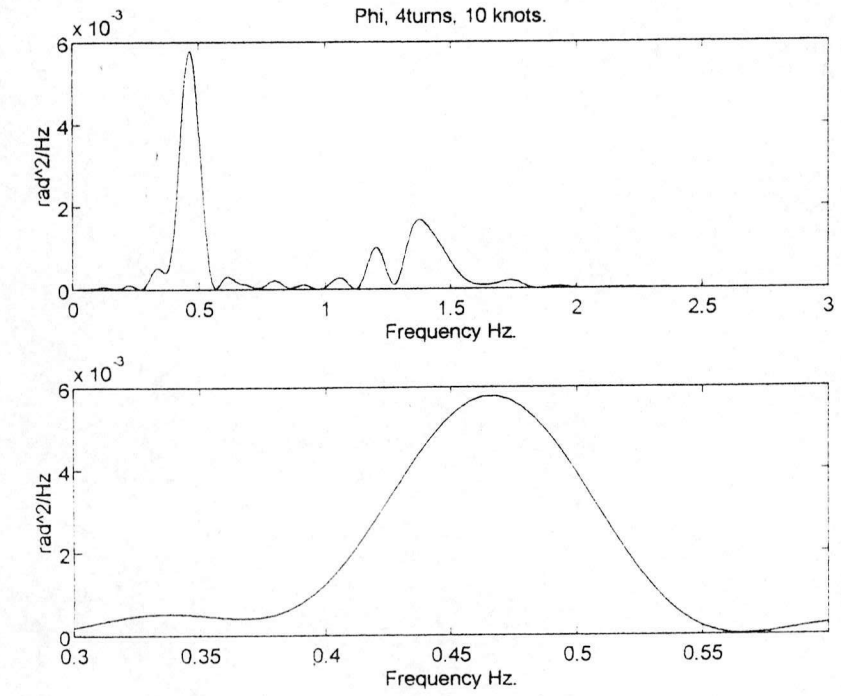

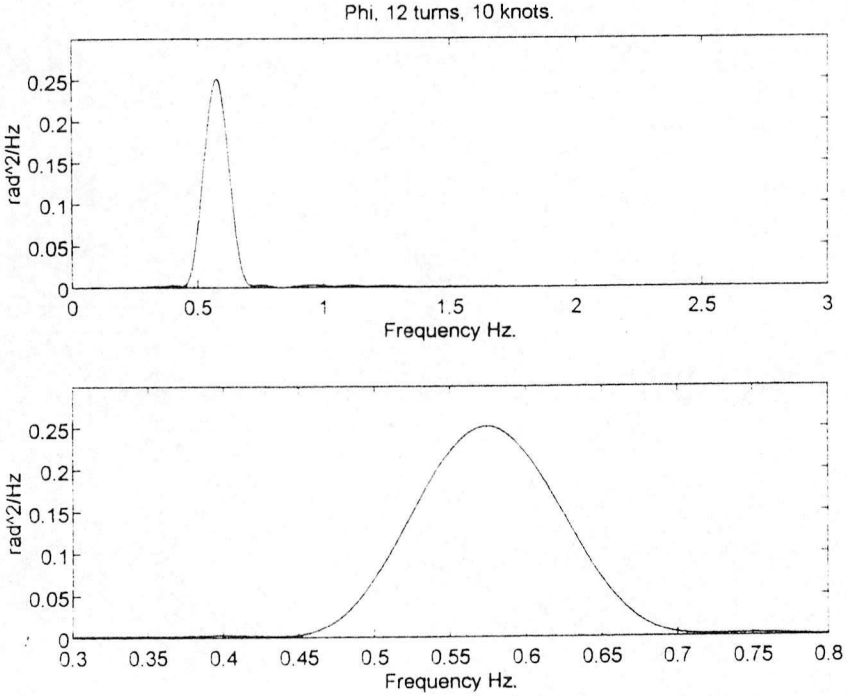

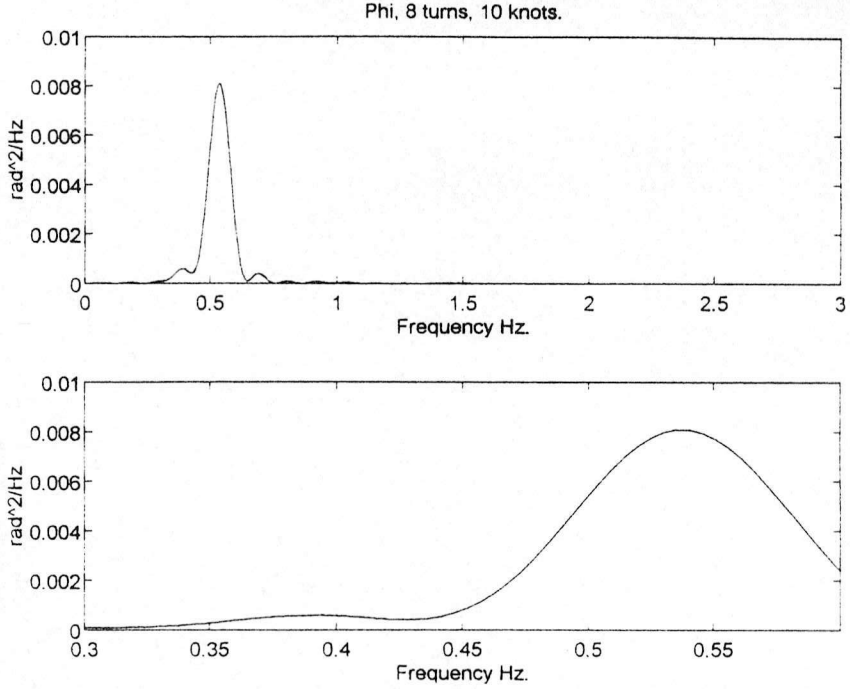

Fig(6.2.12), PSD curves of roll angle, ϕ, 10 knots.

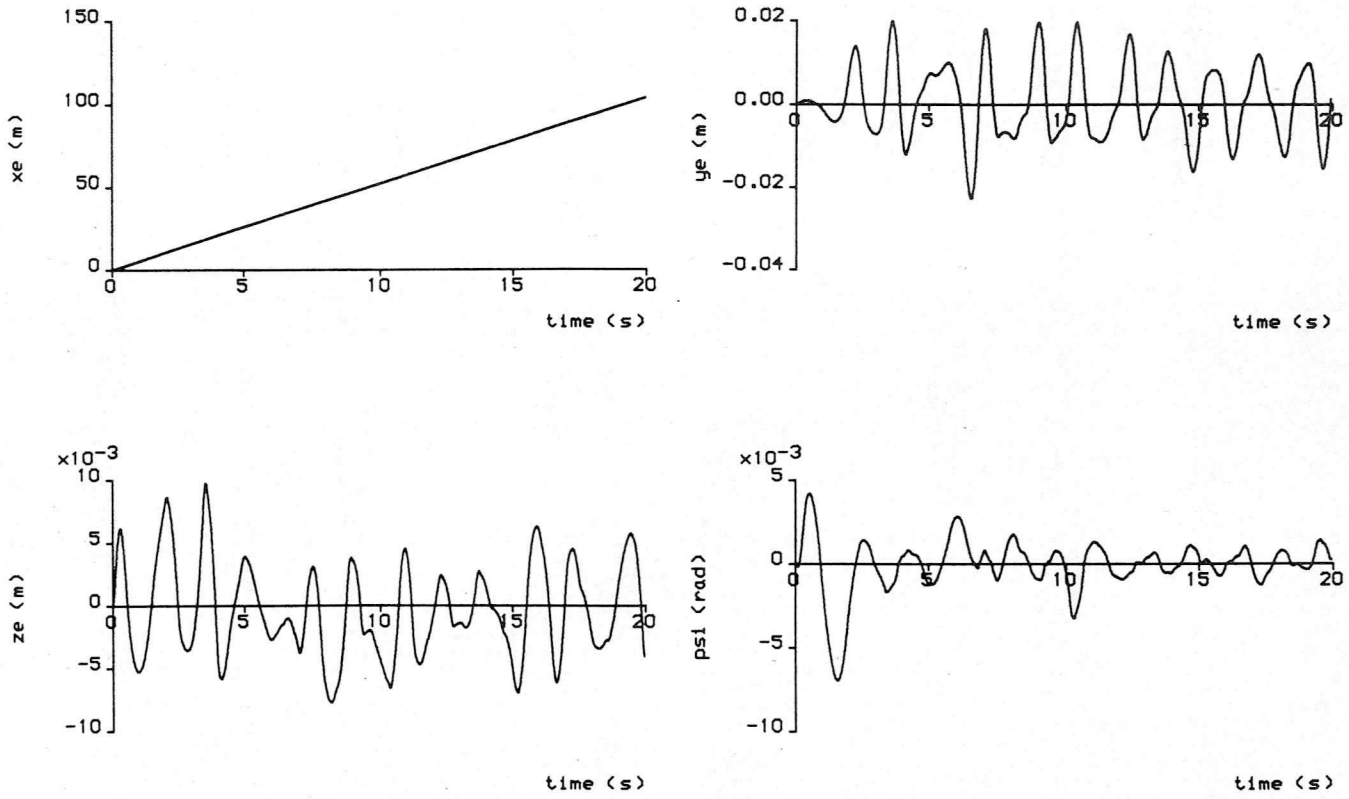

Fig(6.3.1), Performance of the constraint variables in maintaining trim, standard accuracy.

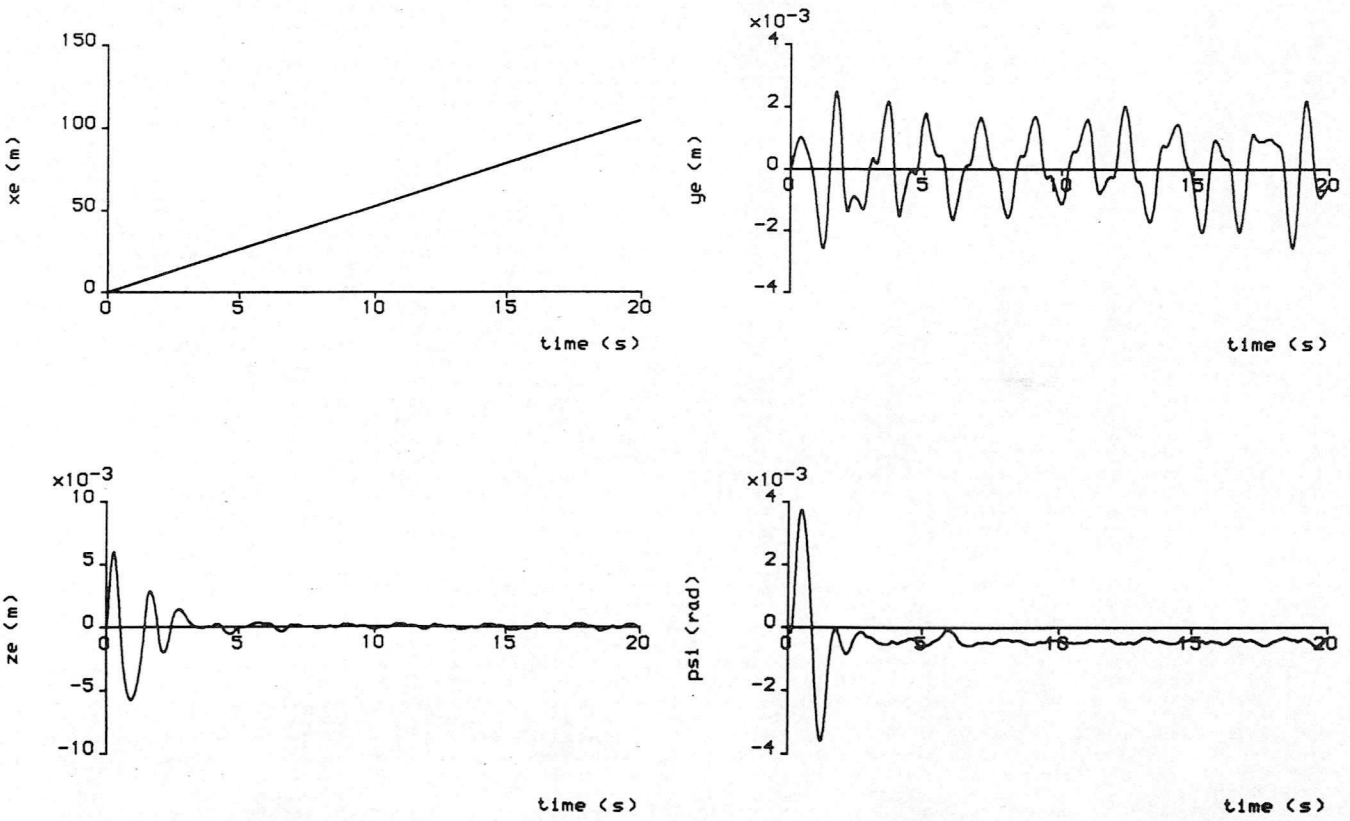

Fig(6.3.2), Performance of the constraint variables in maintaining trim, modified tolerance limits.

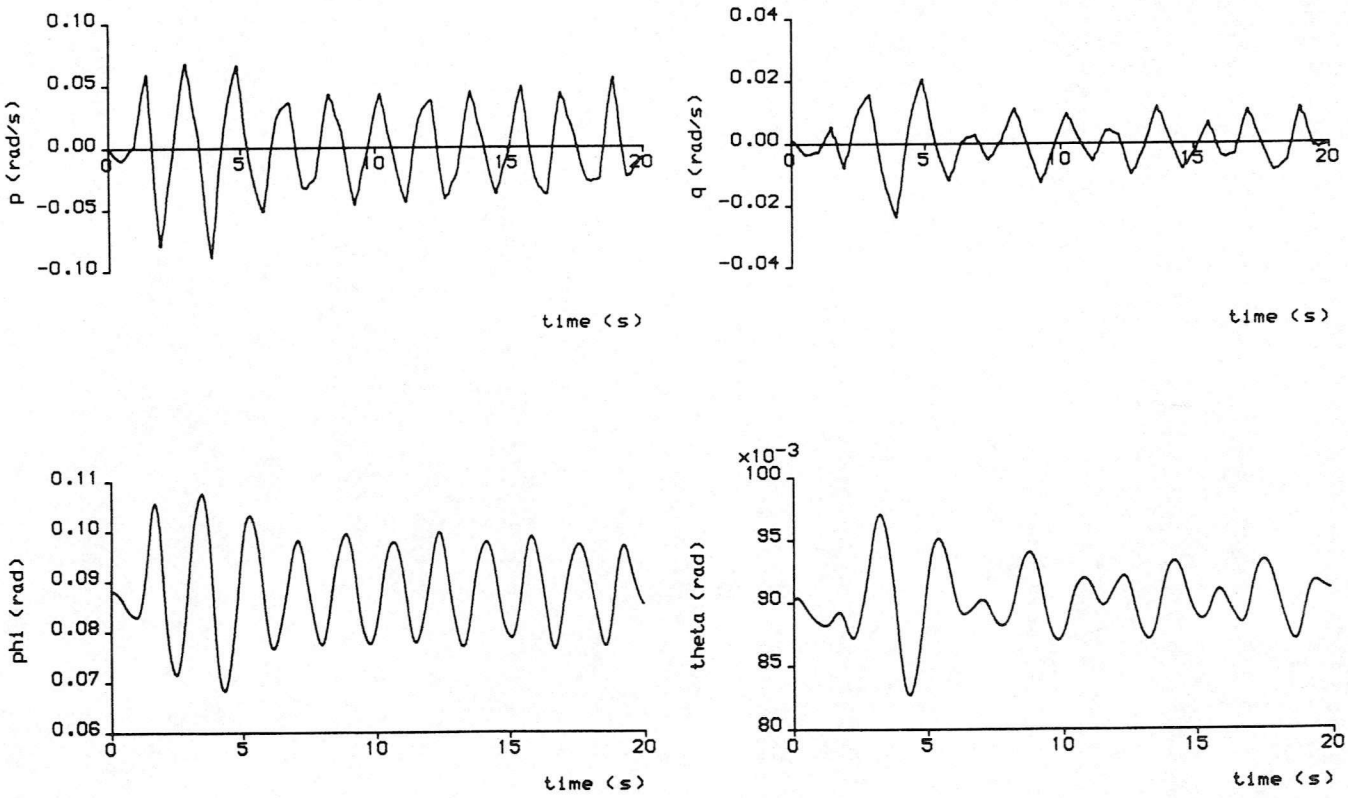

Fig(6.3.3), Constraint oscillations using the modified tolerance limits.

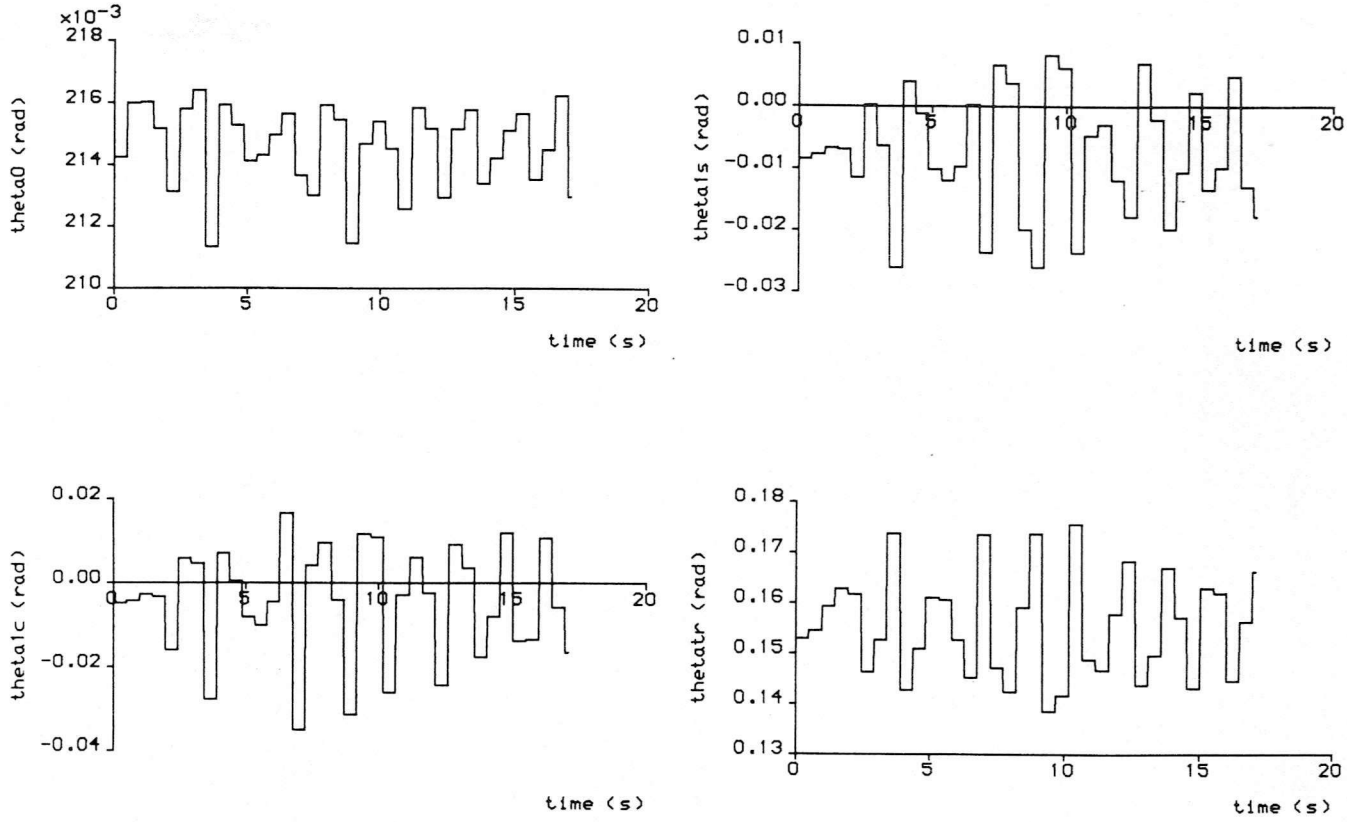

Standard.

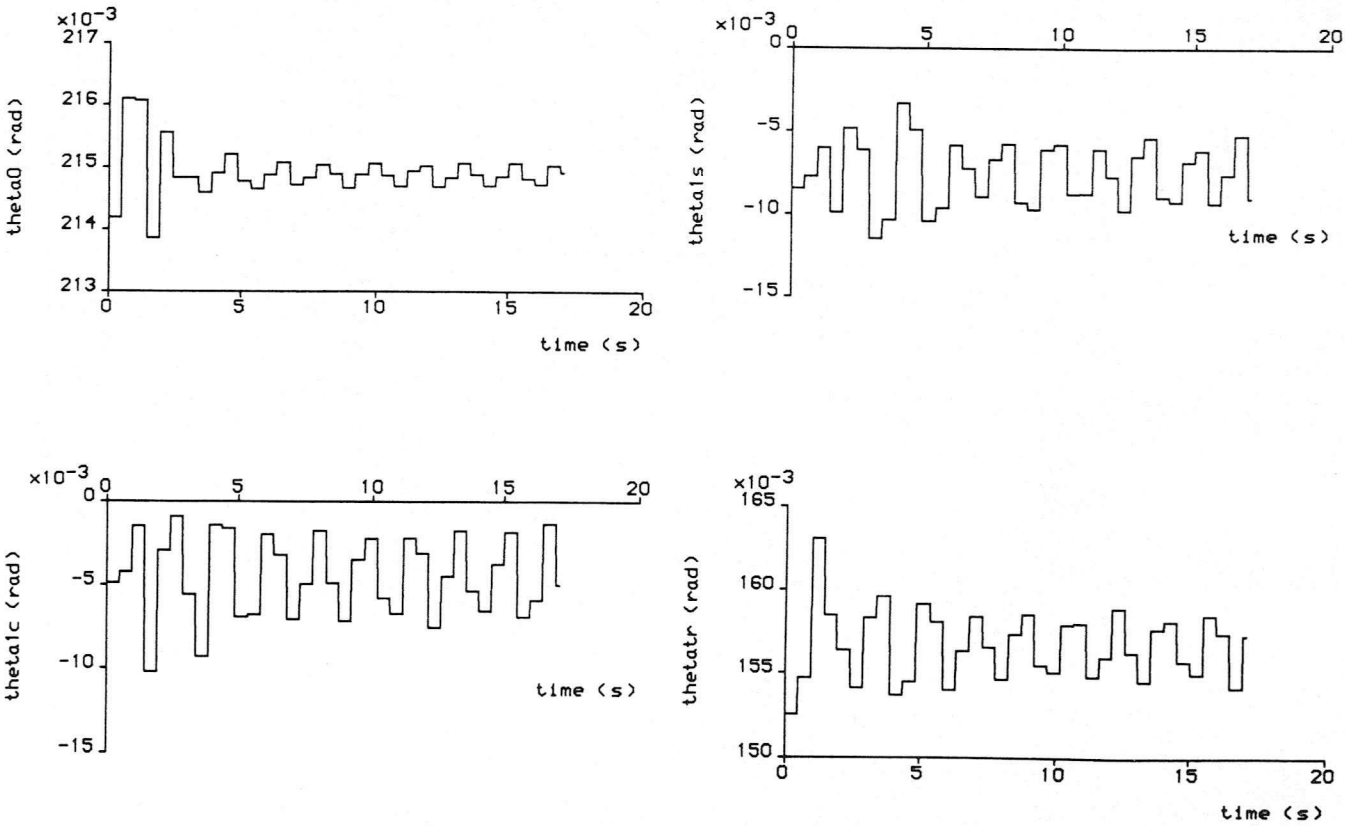

Modified.

Fig(6.3.4), Comparison of the required control deflections for standard and modified tolerance limits.

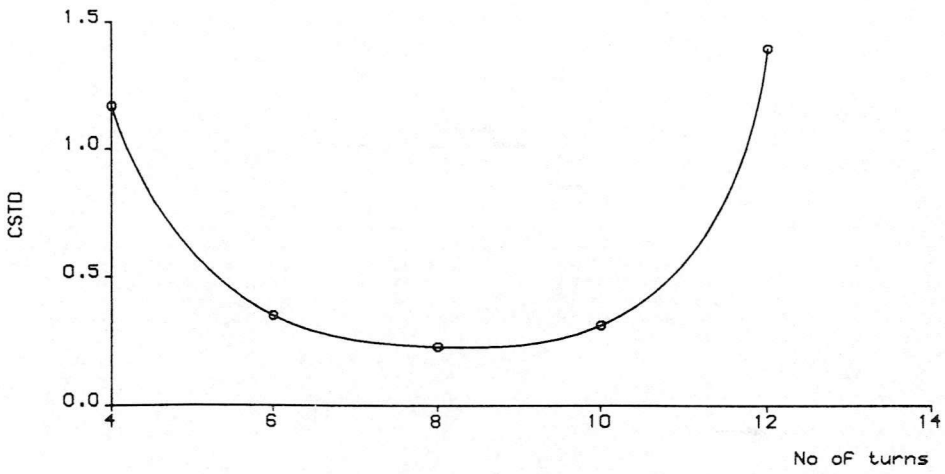

Fig(6.3.5), Cumulative STandard Deviation coefficient vs. interval between succesive control deflections.

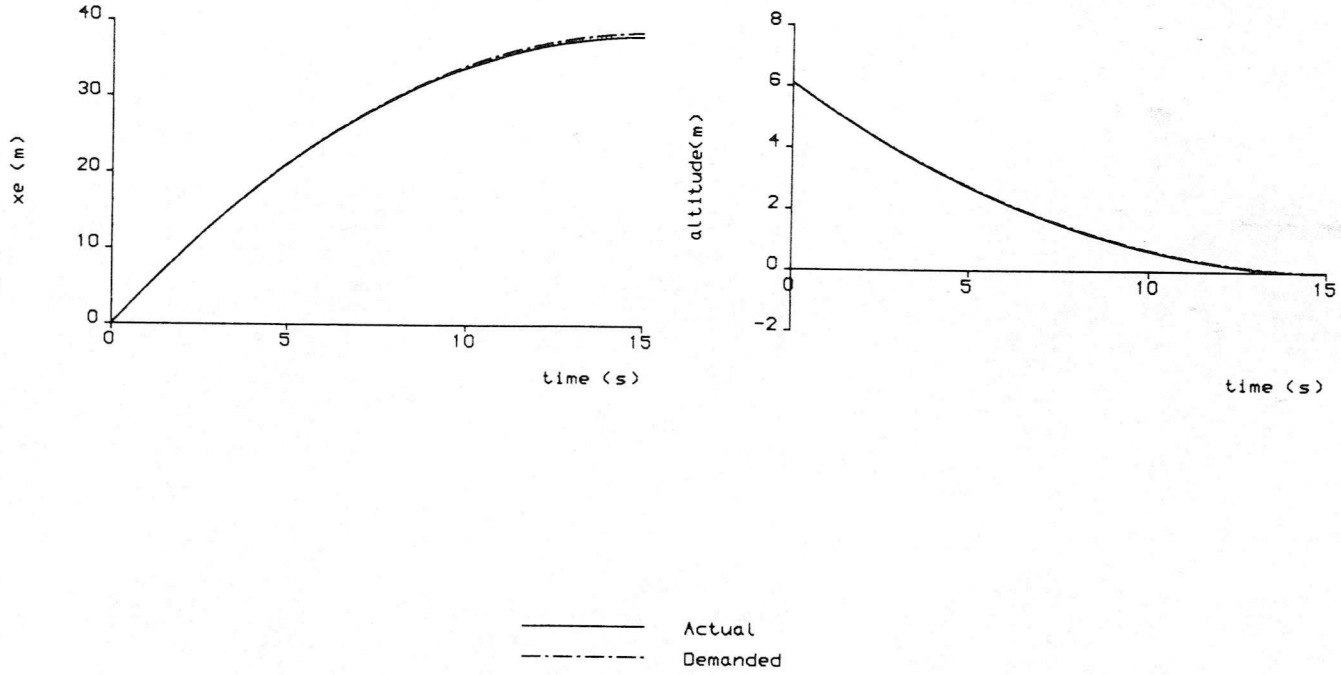

Fig(6.4.1), Control tracking effectiveness for an oil rig platform landing manoeuvre in turbulence.

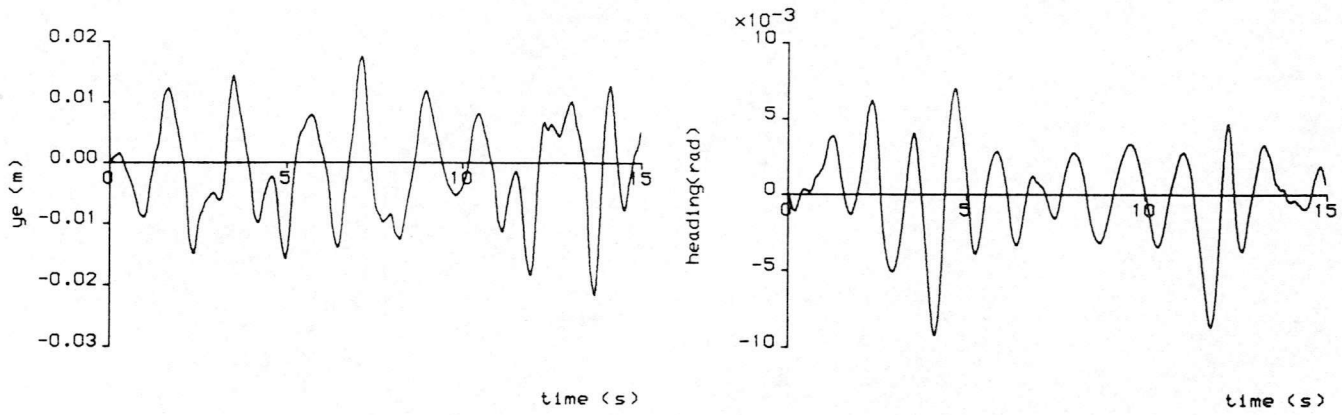

Fig(6.4.2), Lateral / Directional motion for an oil rig platform landing manoeuvre in turbulence.

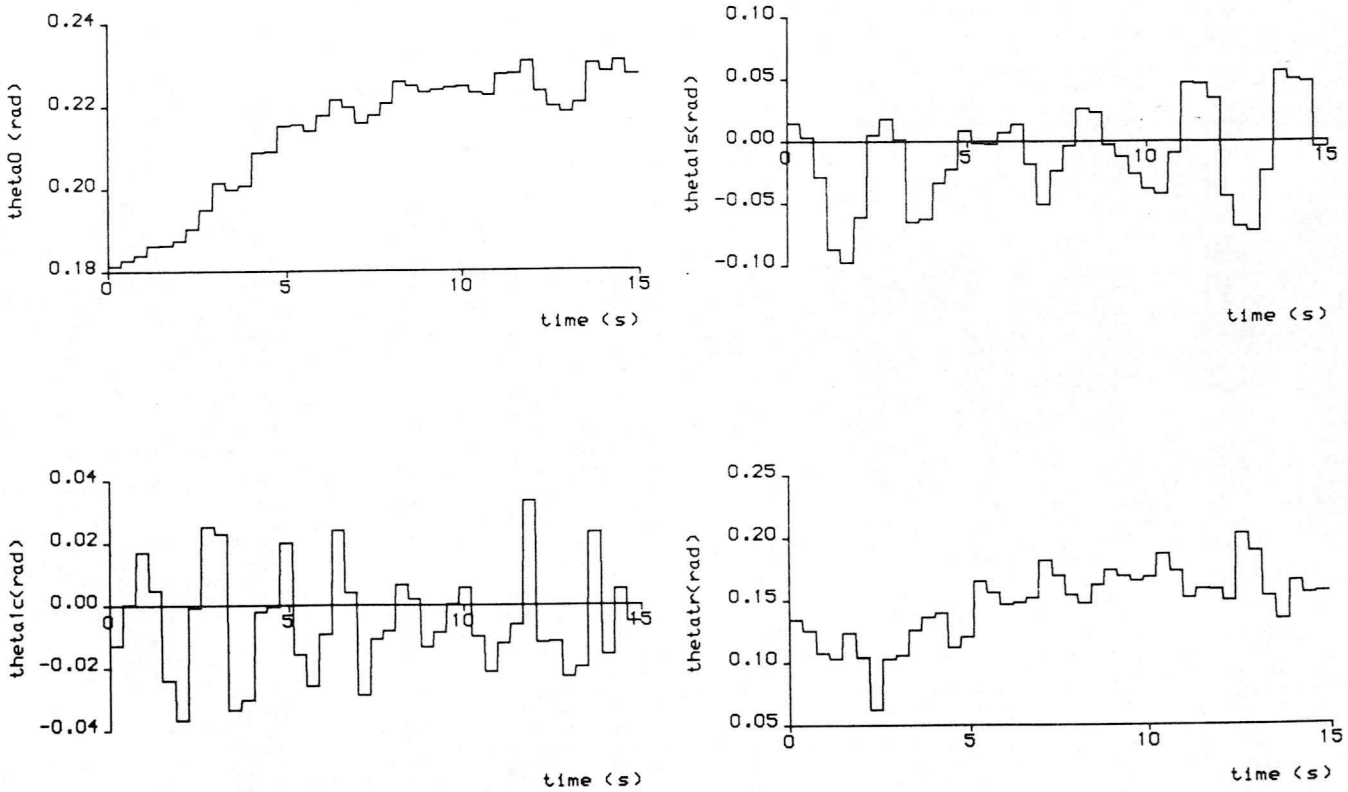

Fig(6.4.3). Control deflections for an oil rig platform landing manoeuvre in turbulence